CHAPTER 7

Induced TGB phases in binary mixtures of achiral hockey stick-shaped and chiral rod-like mesogen

7.1. Introduction

Chirality, *i.e.*, the lack of mirror symmetry is the inherent self-organized property of chiral molecules in liquid crystal (LC) system. Physical properties of nematic and smectic phases formed by chiral molecules differs from the mesophases formed by usual calamitic molecules [1,2]. In addition to normal orientational ordering of LC molecules in the nematic phase, the precessional motion of local director around a helical axis is present in the chiral nematic (*N**) or cholesteric phase. On the other hand, the chirality endorsed in smectic-*A* (Sm-*A*) and smectic-*C* (Sm-*C*) phases are known as smectic-*A** (Sm-*A**) and smectic-*C** (Sm-*C**) [3] phases. Such a combined molecular organization acts as an external field to the system and hence establishes some typical para-electric, ferroelectric and anti-ferroelectric mesophases in LC compounds. Due to the presence of supramolecular helicity, development of several novel thermodynamic phases along with beneficial electro-optic effects of such materials make them advantageous in smart display devices [4-12] and electro-optic technological appliances [13-17].

In chiral LC system, variety of new mesophases such as blue phase (BP) [18,19], chiral line liquid (N_L^*) phase [20,21], twist grain boundary (TGB) [22,23] phase etc. have drawn the attention of the researchers in the last few decades. All these phases are thermodynamically distinct phases of highly chiral compounds, arises in a small temperature range. TGB phases are developed due to competition between helical superstructure of molecular director and positional ordering of smectic layers. The reason for the existence of different TGB phases is that the direct transformation from highly twisted *N** to smectic phases cannot occur in a continuous way as the cholosteric twist of the director is incompatible to form the smectic layer structure. Therefore, encompassing both the structural features reveals a frustrated TGB phase in which locally ordered smectic slabs are separated by grain boundaries which in turn consist of a lattice of screw dislocations and the corresponding helix axis

is perpendicular to the smectic layer normal (Fig. 1.11 in chapter 1). It was theoretically predicted by Renn and Lubensky [1,24] that the TGB phases are identical to the Abrikosov's triangular flux vortex lattice phase of type-II superconductors in an external magnetic field. In case of TGBA phase, the orientation of the molecules within each slab is similar to regular Sm-*A* phase, first observed by Goodby *et al.*[2,25], while the molecular orientation within the slabs of the TGBC phase is tilted as like Sm-*C* phase [24,26]. On the other hand, TGBC* phase comprises of smectic slabs with Sm-*C** orientation of the molecules thereby possess two orthogonal helix axis. Although the TGB phases are generally found in some pure compound having lower pitch length or high chirality in nature, some binary LC mixtures also exhibit the same [27-31]. Notably, the stability of these TGB phases is generally observed in a small temperature range.

The structural features of the molecule have a crucial role to favor the complex orientation in TGB phases. Apart from the typical rod-like molecules, TGB phases has also been found in some pure bent-core mesogens with chiral chain [32,33] and also in some mixtures of chiral compounds with achiral bent-core mesogens [34,35]. The bent-core mesogens have shown global interest in LC community, as they exhibit exceptional structure-induced mesomorphic behavior and unconventional mesophase sequences. Some of the bent-core mesogens are found to possess both spontaneous polarization and biaxiality in orthogonal (Sm-*A*) [36,37] and tilted smectic (Sm-*C*) [38,39] phases. Additionally, the bent-core mesogens reveal some intriguing properties such as giant flexoelectricity [40,41], unique rheological properties [42,43], a considerable Kerr effect [44], unprecedented behavior of electroconvection patterns [45-47], polar switching behavior and structural layer chirality [48-50] due to the presence of bent-shaped unit in the molecular conformation. On the other hand, the asymmetrically configured hockey-stick shaped liquid crystals possess a variety of combinational properties of both symmetric bent-core and

calamitic compounds. For several hockey stick-shaped compounds, no feasible polar character has been found from the electro-optical measurements [51,52]. However, there are also contradictory evidences of low, but clearly measurable value of spontaneous polarization in freestanding films formed by hockey stick-shaped liquid crystals [53,54]. Therefore, the polar character of such compounds is still under investigation. It can be assumed that mixtures of bent-core compounds with the chiral mesogenic system may either influence the polar property of the mixture or may induce atypical mesophases like BP, TGB phases. Till date, a number of chiral-achiral mixtures have been reported to exhibit induced frustrated mesophases. Several physical properties have also been determined in these phases to understand the proper molecular architecture and associated behavior [19,55-58]. The actual process of formation of frustrated structure in such complicated system is still not been properly understood which necessitates further experimental investigations.

In this chapter, two wide temperature ranged TGB phases – TGBA and TGBC* have been observed in a binary system consisting of highly tilted chiral ferroelectric rod-like compound, (S)-(+)-4′-(ω-alkanoyloxy) alkoxybiphenyl-4-yl 4-(1-methylheptyloxy) benzoates (*n*H*m*R), with $n = 2$, $m = 6$ and an achiral hockey stick-shaped compound, namely 4-(3-n-decyloxy-2-methyl-phenyliminomethyl) phenyl 4-n-dodecyloxy cinnamate (H-22.5). Different optical, dielectric and electro-optical investigations have been performed for these binary chiral-achiral mixtures and discussed the possible outcomes in the viewpoint of perturbation introduced by the achiral hockey stick-shaped compound.

7.2. Materials

The investigated host chiral ferroelectric liquid crystal belongs to the homologous series of (S)-(+)-4′-(ω-alkanoyloxy) alkoxybiphenyl-4-yl 4-(1-methylheptyloxy) benzoates (*n*H*m*R) with $n = 2$, $m = 6$ [59], obtained from the Institute of Chemistry, Military University of Technology, Warsaw, Poland and

the guest hockey stick-shaped liquid crystal compound, 4-(3-n-decyloxy-2-methyl-phenyliminomethyl) phenyl 4-n-dodecyloxy cinnamate (H-22.5) [60], discussed earlier in chapter 6, has been used to formulate the investigated mixtures. The structural formulae and transition scheme for the compound 2H6R is given in Fig. 7.1.

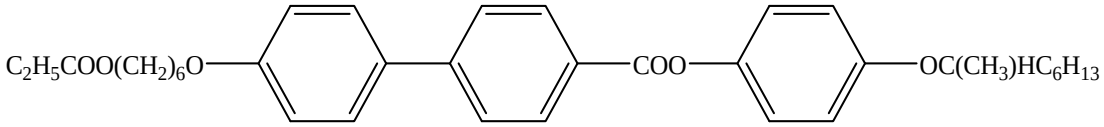

Cr 73.5 ^{o}C (**Sm-*B**$_{hex}$** 66.3 ^{o}C) **Sm-*C**** 90.9 ^{o}C ***N**** 99.9 ^{o}C ***I***

Figure 7.1. Chemical structure and phase behavior of the chiral ferroelectric compound (2H6R).

The rod-like chiral compound (2H6R) possesses a cholesteric or *N** phase (~ 9 ^{0}C) along with a Sm-*C** phase. However, a hexatic Sm-*B**$_{hex}$ phase is also found during cooling cycle [59]. In Sm-*C** phase, the obtained value of the tilt angle is about 33^{o} and spontaneous polarization of about 110 nC/cm^{2} with a helical pitch 400–600 nm. Whereas the asymmetrical hockey stick shaped compound (H-22.5) exhibits the stable phase sequence *I*–*N*–Sm-C_s–Sm-C_a–Cr as being cooled from the isotropic state [60,61], where Sm-C_s and Sm-C_a refer to Smectic-*C* phases having synclinic and anticlinic alignment of the molecules in the adjacent layers. Hence the mixtures of such chiral and achiral, rod-like and hockey stick-shaped compounds with nearly equal clearing temperature are of significant interest to study the resultant mesophase behavior and their physical properties. Three concentrations have been prepared by adding guest hockey stick-shaped compound (H-22.5) in the host chiral ferroelectric compound (2H6R), having mole fractions of H-22.5: $x_{\text{H-22.5}}$ = 0.101, 0.202, 0.306.

7.3. Optical texture and DSC studies

Identification of different liquid crystalline mesophases and corresponding temperature scheme for all the studied mixtures have been

carried out by polarizing optical microscopy and DSC study. The optical textures were observed during cooling cycle of the samples, filled in commercially available ITO coated planar and homeotropically aligned cells of thickness ~ 9 μm.

During cooling from the isotropic phase, all the investigated mixtures exhibit four distinct mesophases. The *N** or cholesteric phase emerges as a first high-temperature mesophase similar to the pure chiral compound 2H6R. Fig. 7.2 represents the optical micrographs for the concentration $x_{\text{H-22.5}}$ = 0.202 in the *N** phase. The appearance of nematic droplets has been noticed at the isotropic to *N** phase transition (Fig. 7.2(a)). However, the cholesteric Grandjean texture (Fig. 7.2(b)) is also observed for the 2H6R compound as well as for the mixture concentration $x_{\text{H-22.5}}$ = 0.306 just after the transition from the isotropic phase. Generally this texture defines a pitch length of the order of a few μm. With lowering of temperature, different types of cholesteric textures appears *viz*. the broken fan-like texture of the short pitch depicted in Fig. 7.2(c), oily streaks texture in Fig. 7.2(d,e), fluctuating color domain cholesteric textures in Fig. 7.2(f,g), a sharp appearance of cholesteric finger in Fig. 7.2(h) and reappearance of oily streaks textures at a lower temperature as illustrated in Fig. 7.2(i) [23,62]. Different color domains in Fig. 7.2(f,g) correspond to different twist states and the "black" domain in Fig. 7.2(g) stands for a quasi-nematic director configuration that can be brought into an extinction position by rotating the sample between crossed polarizers. Specifically, this state is nailed as the twist inversion state [23] where the nucleation and quickly grown up of some color domains can be visualized in all the mixtures. Different chiral compounds and even some binary mixtures are reported to reveal this twist inversion phenomenon [62-67]. Due to existence of the helical superstructure of the *N** phase, its textural appearance and optical properties are quite different from those of usual nematic phases. All these textures in Fig. 7.2(a-i) have been observed in the planar configuration of the sample. In case

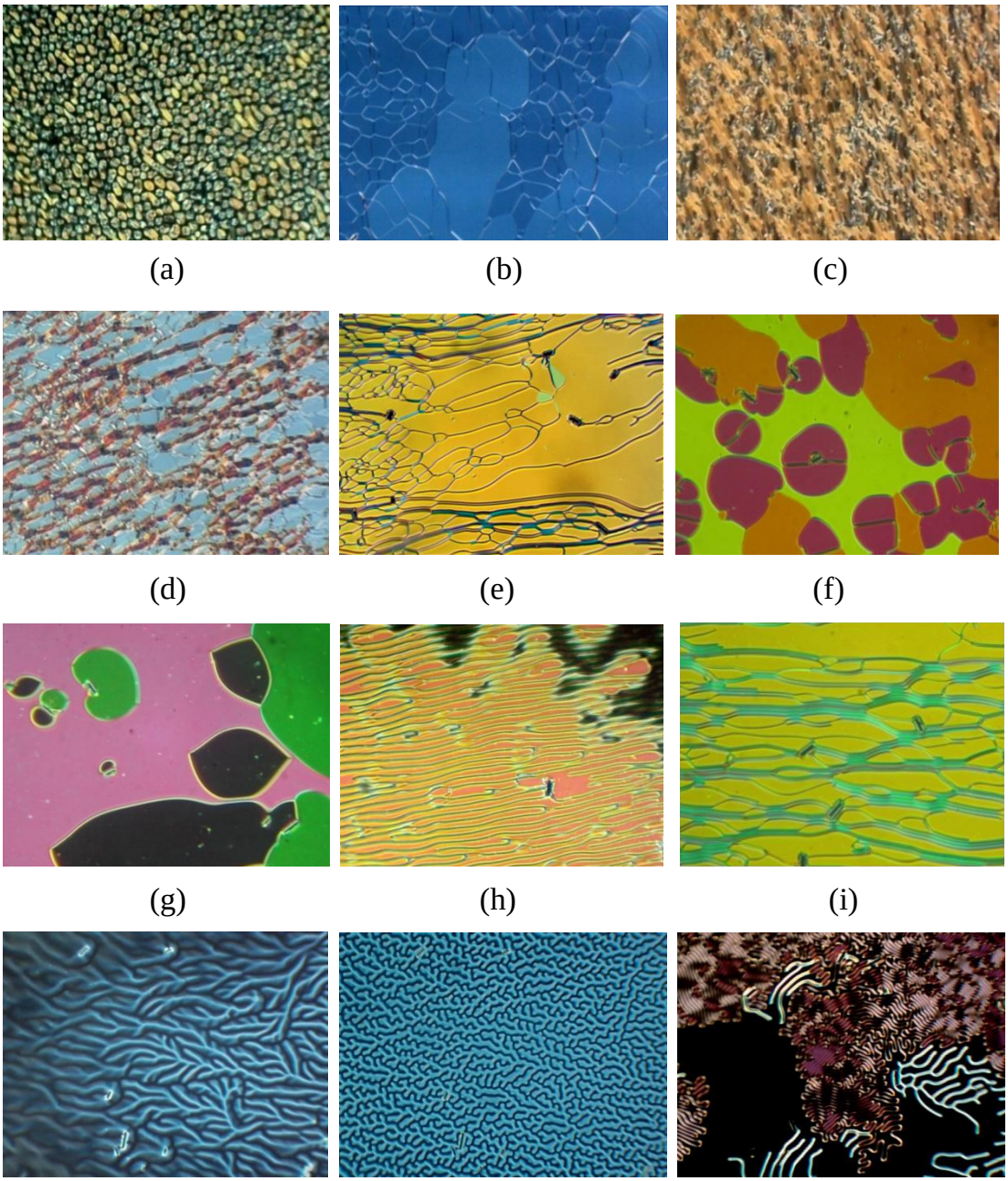

Figure 7.2. Optical textures of *N** phase by lowering the temperature as: (a) nematic droplets at 98.5 ^{o}C, (b) cholesteric Grandjean texture of 2H6R at 98.3 ^{o}C, (c) cholesteric fan-like texture at 98 ^{o}C, (d-e) oily streaks texture at 97.6 ^{o}C and 97.2 ^{o}C, (f-g) color domain texture of different twist and twist-inversion states at 96.8 ^{o}C and 96.6 ^{o}C, (h) texture with cholesteric finger at 96.2 ^{o}C, (i) oily streaks textures appears again at 95.5 ^{o}C, (j-k) texture with cholesteric finger in homeotropic cell at 96.5 ^{o}C, 96 ^{o}C respectively, (l) coexisting of fingerprint texture with cholesteric finger at 94.3 ^{o}C for $x_{\text{H-22.5}}$ = 0.306.

of homeotropic anchoring condition, an optical texture with typical cholesteric fingers has appeared close to the twist inversion temperature of the *N** phase as shown in Fig. 7.2(j,k). The dark areas representing a pseudo-isotropic twisted state for a strong homeotropically aligned sample. A coexistence of fingerprint texture with cholesteric fingers has also been observed for $x_{\text{H-22.5}} = 0.306$ (Fig. 7.2(l)). Black regions of this texture specifying the unwound, non-helical state where the director tends to align parallel to the optic axis in the homeotropic configuration of the sample [23]. Hence, it is an indication of a transition to a mesophase where the molecular director is parallel to the direction of light propagation. All the texture confirms that the cholesteric pitch length of the twisted *N** phase is increasing by lowering the temperature and thereby exhibiting a continuous change of several optical textures with different colors.

The transition from the *N** phase to low-temperature mesophase is characterized by Grandjean type optical textures in planar aligned sample as shown in Fig. 7.3(a-c), while the homeotropically anchoring sample leads to filament type textures as shown in Fig. 7.3(d-f). The optical textures observed in the homeotropic alignment are mostly covered by black (optically isotropic) region. Here the molecular director is oriented in a parallel direction to the optic axis as like homeotropically aligned Sm-*A* phase. However, all of these textures appearing in the present system are the characteristics of the TGBA phase [32,68,69]. Moreover, the theoretical prediction suggesting that the transition from cholesteric to chiral smectic-*C* (Sm-*C**) phases can occur either by first order untwisting of molecular director or by inducing both the TGBA and TGBC* phases [1,26]. Therefore, the presence of higher order pitch length of helix axis and an affinity to form layer structure with the orthogonal Sm-*A* ordering of the molecules gives rise to such frustrated TGBA phase by decreasing the temperature from the *N** phase. Although, this type of frustrated phases is mostly found in a small temperature ranges, but the stability of the present TGBA phase is observed in a broad temperature range (around 5-8 ^{o}C).

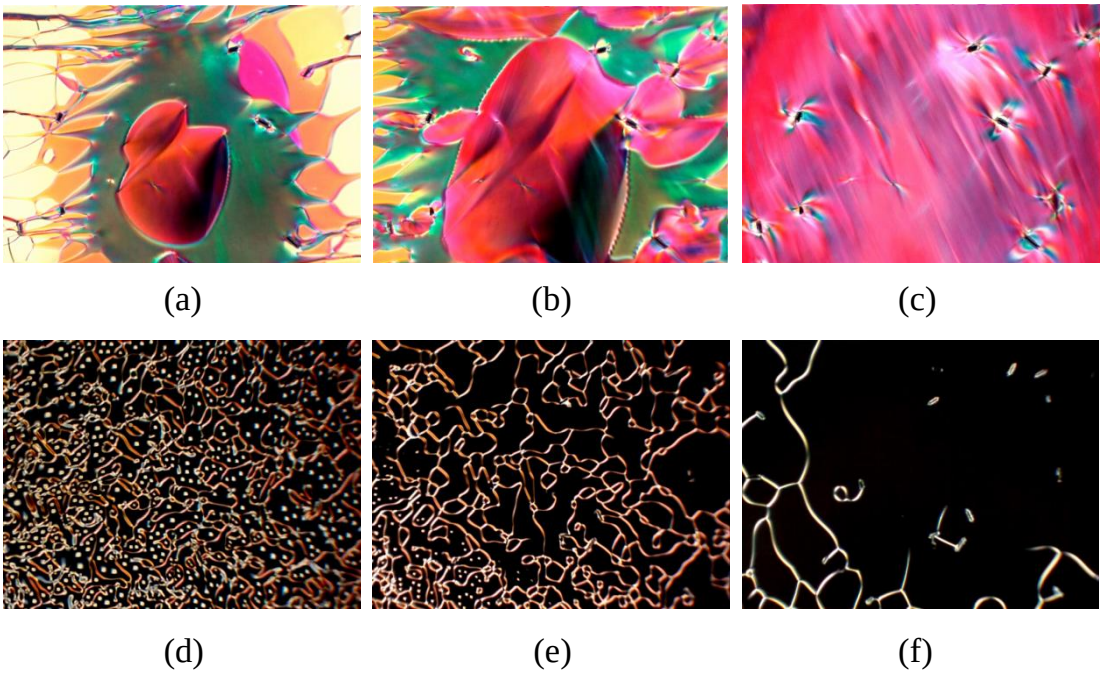

(a) (b) (c)

(d) (e) (f)

Figure 7.3. Optical textures of TGBA phase by lowering the temperature as follows: (a-b) transition from *N** to TGBA phase in planar configuration at 93.3 ^{o}C and 93.25 ^{o}C, (c) Grandjean texture of TGBA phase at 92.1 ^{o}C, (d-e) filament texture at the transition from *N** to TGBA phase in homeotropic configuration at 93.25 ^{o}C and 93.2 ^{o}C, (f) appearance of black domain for TGBA phase at 93 ^{o}C.

Further lowering the temperature, optical textures of the TGBA phase modifies to a square grid pattern across the Grandjean texture in planar boundary condition. The manifestation of such square grid texture is the characteristic features of TGBC* phase [70,71]. Fig. 7.4(a-c) illustrates the micrographs in the TGBC* phase in planar configuration and Fig. 7.4(d-e) represents the same in homeotropic alignment. The appearance of such square grid pattern in the TGBC* phase may be a consequence of the undulation of the smectic slabs [72]. However, according to the model of Galerne [73], which is an extended model of Renn *et al.* [26], this type of cross grid structure develops due to the separation of helislabs by disclination lines. Since the pure compound 2H6R possess Sm-*C** phase, a significant influence of the molecular tilt as well as precessional approach is responsible to develop this frustrated undulated TGBC* phase in the mixtures in which the TGB helix is oriented

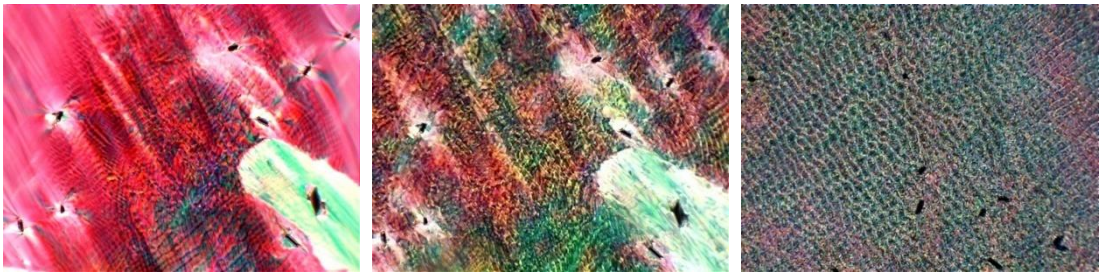

(a) (b) (c)

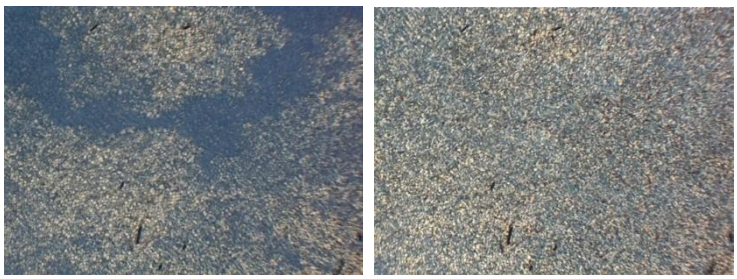

(d) (e)

Figure 7.4. Optical textures of TGBC* phase by lowering the temperature: (a) appearance of cross-grid pattern in planar aligned Grandjean texture of TGBA phase at 84.6 ^{o}C, (b) well-formed texture of TGBC* phase at 84.5 ^{o}C, (c) appearance of modulated texture of TGBC* phase at 80 ^{o}C for $x_{\text{H-22.5}}$ = 0.306, (d) transition to TGBA–TGBC* phase at 84.8 ^{o}C in homeotropic cell, (e) well-formed TGBC* phase texture at 82 ^{o}C in homeotropic cell.

perpendicular to the bounding plates, *i.e.*, parallel to the direction of the light propagation. Therefore, the square grid structure is the result of the mutual configuration of the helical director within the individual Sm-*C** blocks where the helix axis of all the slabs being in the plane of the substrate and mutually perpendicular in adjacent smectic blocks [32,74-76]. The temperature stability of this mesophase has found to be quite large (maximum 37.5 ^{o}C for $x_{\text{H-22.5}}$ = 0.202) compared to that of the TGBA phase.

The fourth mesophase, *i.e.*, the Sm-B^*_{hex} phase has been observed with the appearance of a mosaic texture in planar anchoring cell at a low temperature for all the investigated mixtures. In both the configurations, almost similar textures are found in the mixtures and pure compound 2H6R. Fig. 7.5 (a) and Fig. 7.5(b) illustrate the textures of Sm-B^*_{hex} phase in planar anchoring condition for the pure compound and the homeotropic anchoring texture for the

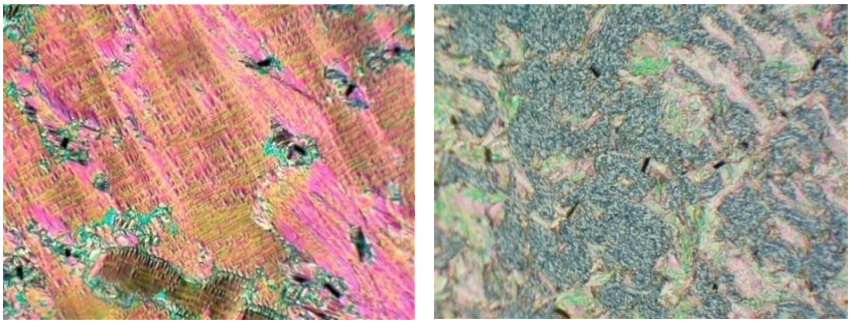

(a) (b)

Figure 7.5. Optical textures of lower temperature Sm-B*$_{hex}$ phase at (a) 50 ^{o}C for pure 2H6R compound in planar cell, (b) 48.6 ^{o}C for $x_{H\text{-}22.5}$ = 0.202 in homeotropic alignment.

mixture concentration $x_{H\text{-}22.5}$ = 0.202. This type of mosaic texture demonstrates a smectic phase with hexatic order in a most stable configuration. Moreover, the optical textures reveal some small domains with uniform optical appearance, separated by domain boundaries. In this case, the smectic layers are oriented in a perpendicular direction to the substrate plane and the director in each domain is oriented along a particular direction, which varies from domain to domain. This causes a uniform optical appearance within a single domain.

Furthermore, the phase transition temperatures associated with all the mesophases were determined by investigating the differential scanning calorimetry (DSC) using Pyris Diamond Perkin-Elmer 7. Measurements were carried out by taking the sample (~ 4 mg) in a hermetically sealed aluminium pan in a nitrogen atmosphere. The representative thermogram for the mixture $x_{H\text{-}22.5}$ = 0.202 during heating and cooling cyclen (at a rate 10 ^{o}C min^{-1}) is presented in Fig. 7.6. DSC thermogram shows sharp peaks at the transitions of the investigated mixtures and the corresponding amount of enthalpy change [ΔH] (kJ/g) has been calculated from the experimental curve. The phase transition scheme obtained from DSC study is summarized in Table 7.1 for the mixture $x_{H\text{-}22.5}$ = 0.202. All the phase transition temperatures were easily been detected (except the N*–TGBA transition) from the DSC study and found to

reveal a good agreement with the same obtained from polarizing optical microscopy. Therefore, all the mixtures exhibit the following phase sequence: *I*–*N**–TGBA–TGBC*–Sm-*B**$_{hex}$. Among all the mesophases, TGBC* phase sustains in a quite large temperature range which is very rare and the bend-shaped molecular structure of hockey stick-shaped compound is assumed to be responsible for the induction of these (TGBA and TGBC*) frustrated mesophases.

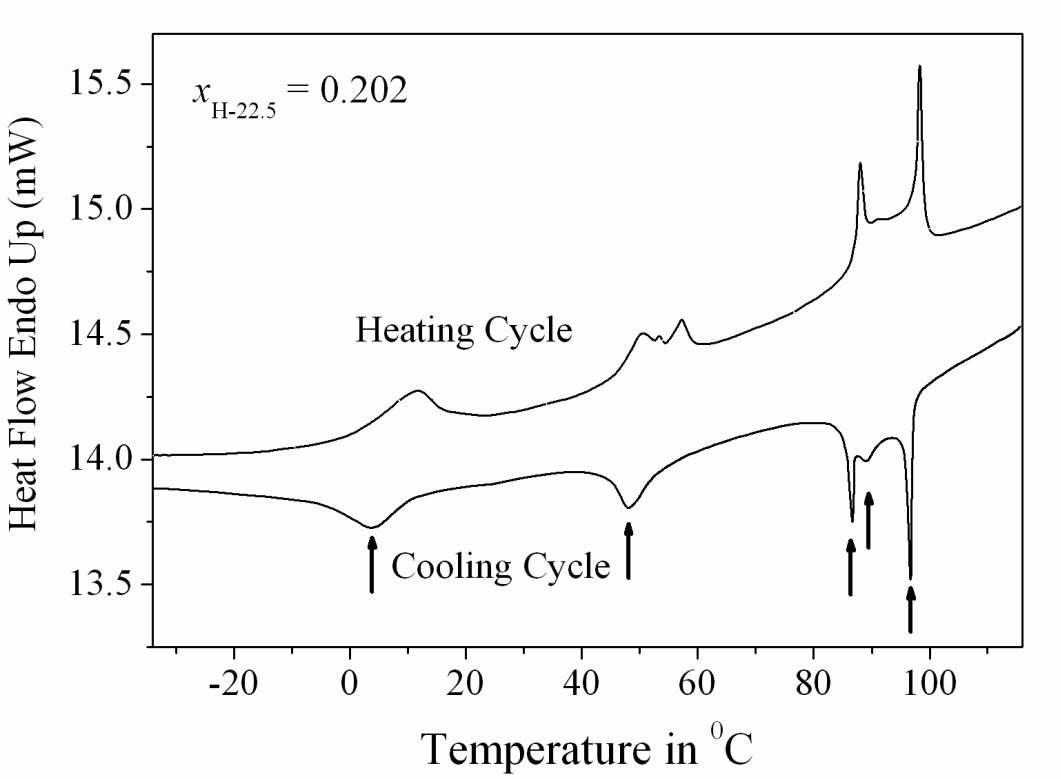

Figure 7.6. DSC thermograms on both heating and cooling cycle for the mixture concentration $x_{H\text{-}22.5}$ = 0.202.

Table 7.1. Sequence of phases, temperature schemes (^{o}C) and transition enthalpies [ΔH (J/g)] during cooling cycle for the mixture $x_{H\text{-}22.5}$ = 0.202.

Cr	←	**Sm-*B**$_{hex}$**	←	**TGBC***	←	**TGBA**	←	***N****	←	***I***
•	4.2 [-4.5]	•	49.1 [-2.2]	•	86.6 [-1.5]	•	90.5 [-0.4]	•	96.4 [-1.4]	•

7.4. Phase diagram

The partial phase diagram of the binary system consisting of H-22.5 and 2H6R for three different concentrations along with the pure compound 2H6R has been illustrated in Fig. 7.7(a). The transition temperatures are based on the values obtained from the polarizing optical microscopy and DSC study. The pure hockey stick-shaped compound H-22.5 shows the stable phase sequence *I*–*N*–Sm-C_s–Sm-C_a–Cr as being cooled from the isotropic state [60], where Sm-C_s and Sm-C_a refer to Smectic-*C* phases having synclinic and anticlinic alignment of the molecules in the adjacent layers. On the other hand, the pure chiral ferroelectric compound (2H6R) exhibits the *N** and Sm-*C** phases in conjunction with hexatic smectic (Sm-B^*_{hex}) phase [59].

A small amount of guest H-22.5 compound has been added to the host mesogenic chiral ferroelectric compound to prepare the mixtures. In these binary mixtures, significant focus has been taken on the region where the concentration of the guest compound (H-22.5) is much less compared to that of the chiral compound (2H6R). In this regard, the presence of the bent-shaped mesogenic compound highly interrupts the chiral environment of the host mesogen and responsible to develop a couple of TGB phases. Noticeably, the suppression of Sm-*C** phase of the pure compound has been found along with a significant induction of TGBA and TGBC* phases in all the mixtures. However, the estimated temperature range of the *N** phase monotonically decreases by increasing the amount of hockey stick-shaped compound in the host mesogenic system. The variation of the *N**, TGBA and TGBC* phase ranges against molar concentration is also presented in Fig. 7.7(b). By increasing the amount of H-22.5 compound enhances the width of TGBC* phase with a relatively small change in the width of *N** and TGBA phases. The width of *N** phase decreases from a value 9 ºC (for pure 2H6R) to a value of 5 ºC for the mixture concentration $x_{H\text{-}22.5} = 0.306$, while the temperature ranges of TGBA and TGBC* phases follow a non-linear trend opposite to each other

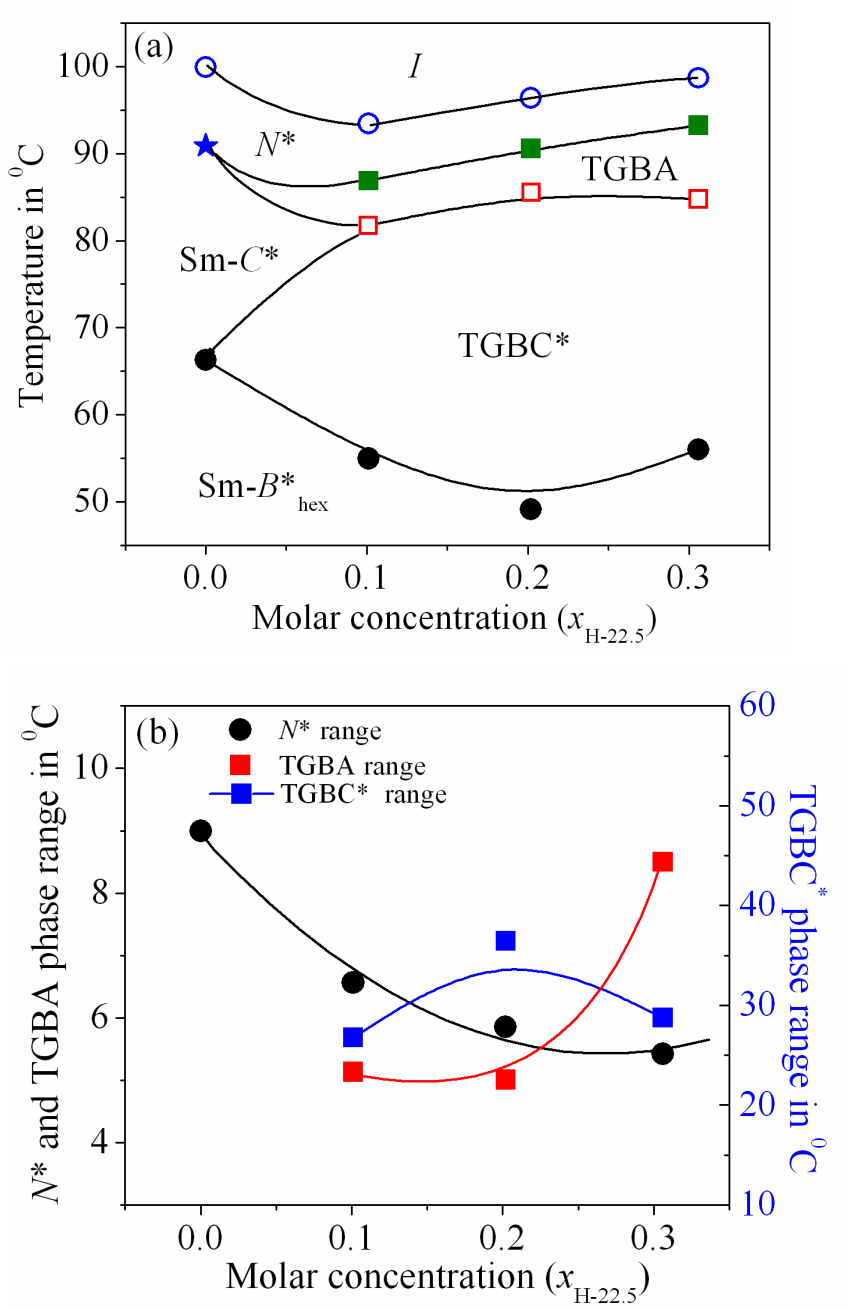

Figure 7.7. (a) Phase diagram for the composite mixture consisting of H-22.5 and 2H6R. $x_{H\text{-}22.5}$ denotes the mole fraction of H-22.5. *I* - isotropic phase, *N** - chiral nematic phase, Sm-*C**- chiral Sm-*C* phase, TGBA- frustrated smectic-*A* phase and TGBC*- frustrated smectic-*C* phase. ○: *I*–*N** transition temperature; ■: *N**–TGBA transition temperature; □: TGBA–TGBC* transition temperature; ★: *N**–Sm-*C** transition temperature; ●: TGBC*–Sm-B^*_{hex} phase transition temperature. (b) Variation of *N**, TGBA and TGBC* phase range with concentration for the present system. Solid lines are drawn for guidance to the eye.

with the variation of molar concentration. However, the temperature stability of the TGBA phase is quite smaller in comparison to the TGBC* phase, although it increases by increasing the concentration of the hockey stick-shaped mesogen. Besides, the maximum range of TGBC* phase has been found around 37 ºC for $x_{\text{H-22.5}} = 0.202$ which is quite large for frustrated phases.

7.5. Optical transmission intensity study

The temperature-dependent optical transmission intensity, measured by the high-resolution optical transmission (OT) technique [77-80] are depicted in Fig. 7.8(a-d) for all of the studied mixtures including the pure chiral compound (2H6R). The measurement has been carried out by taking the samples in ITO coated commercial cells of thickness 9 μm in both the planar (HG) and homeotropic (HT) configurations. In this study all the phase transition temperatures are clearly been detected for both the cell configurations.

The obtained results reveal that the transmitted intensity value increases at the *I*–*N** phase transition for all the investigated samples in both the planar and homeotropic cell configurations due to the increase of order parameter. For the pure compound (2H6R), the intensity value has been found to decrease sharply at the *N**–Sm-*C** phase transition. However, at the *N**–TGBA phase transition a pronounce change in the transmission intensity is observed for all the studied mixtures. On entering the TGBA phase, the intensity data exhibit a sharp enhancement followed by a decrease just before the phase transition and this change is well recognized in HT configuration compare to that of the planar alignment. Noticeably, this minimum intensity value close to the *N**–TGBA phase transition has also been observed in optical texture which appears as black in HT cell at the twist inversion temperature as shown in Fig. 7.2 (l). As the pitch length of the cholesteric phase monotonically increases by decreasing the temperature, helix is continuously unwinding in this mesophase. Probably, due to the occurrence of twist inversion phenomena in the present

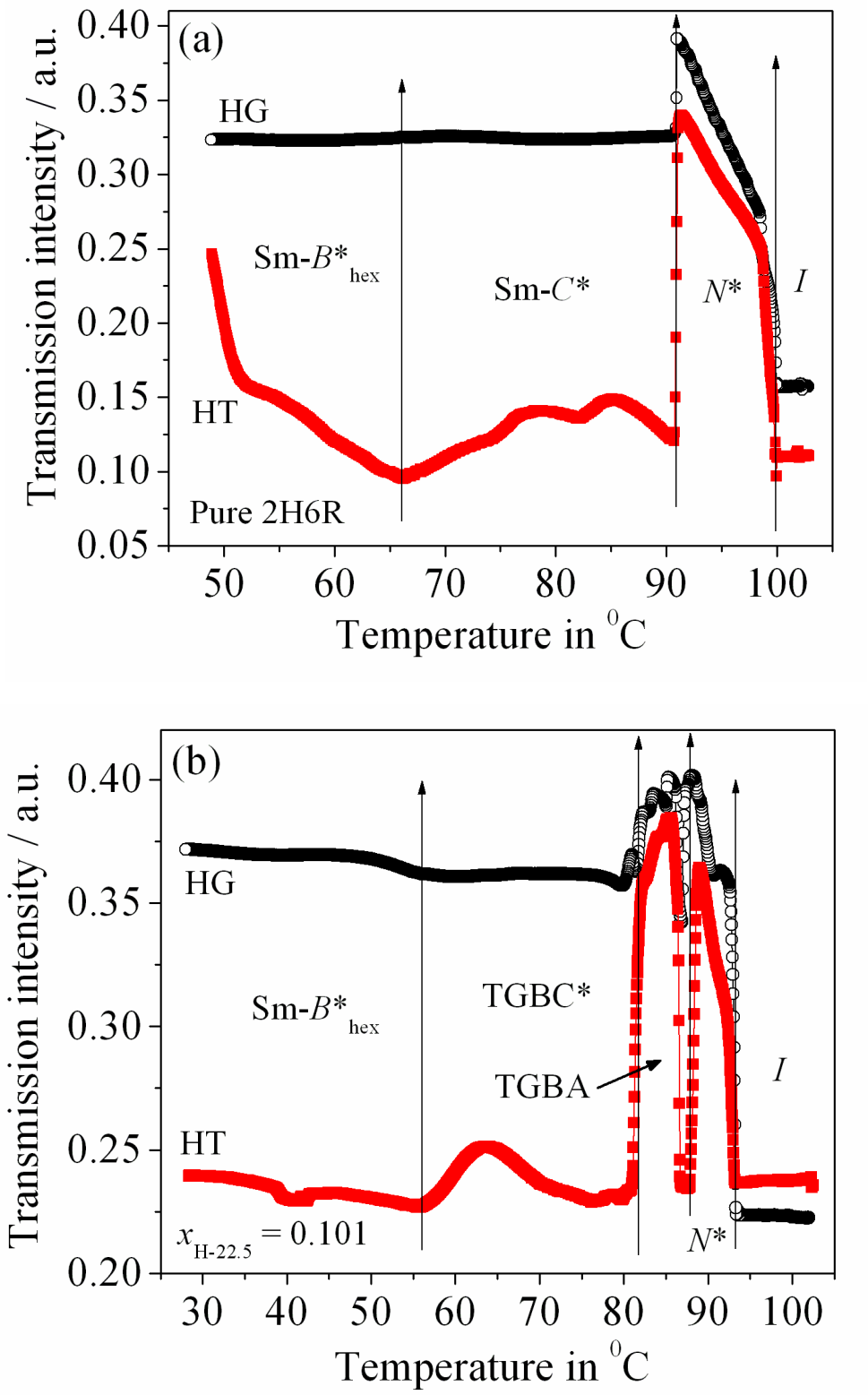

Figure 7.8. Temperature-dependent measured optical transmission intensity for compound (a) 2H6R, and (b) $x_{H\text{-}22.5}$ = 0.101 respectively in planar (open circle) cell and also homeotropic (closed square) cell configuration. Vertical arrows represent the corresponding phase transition.

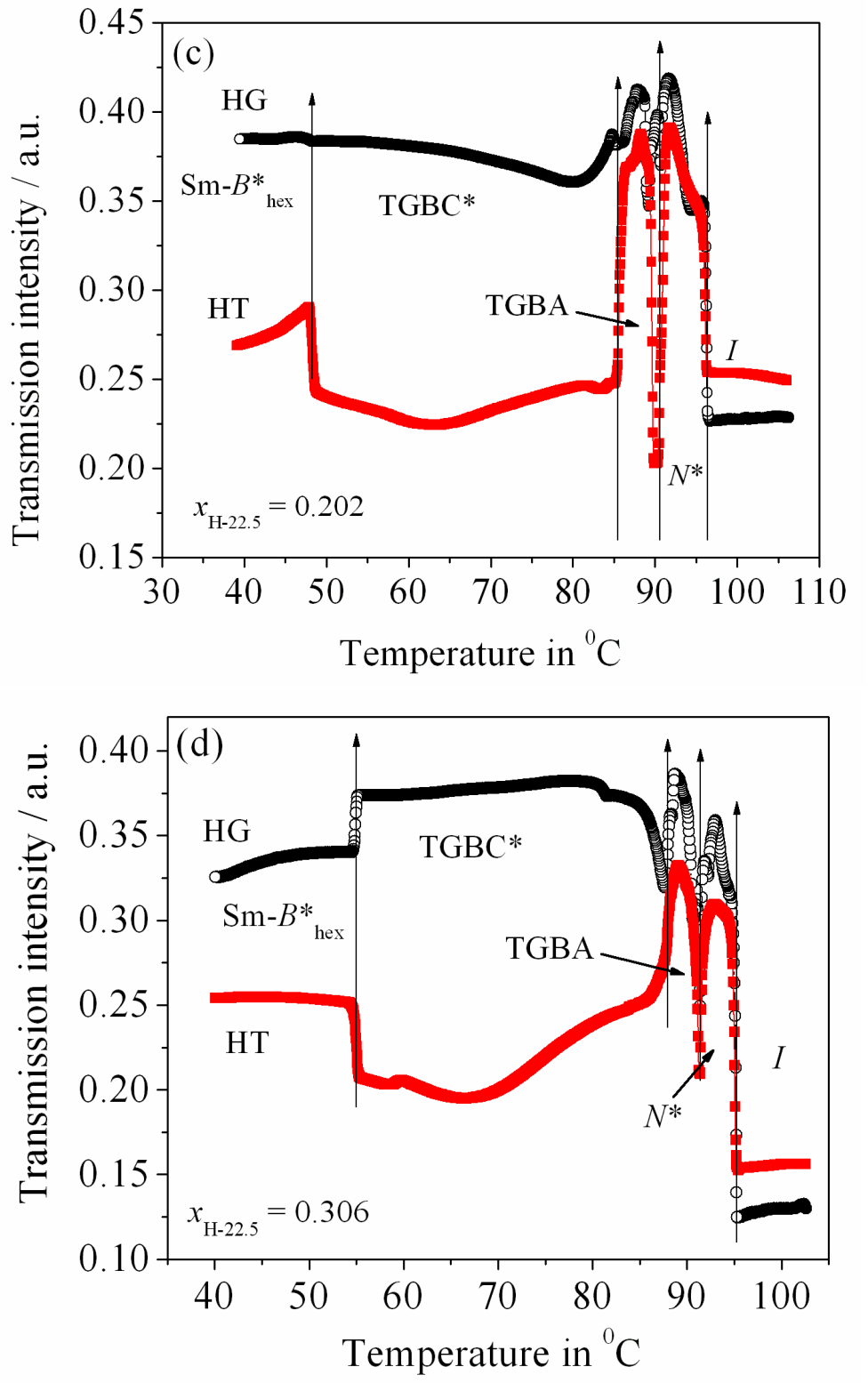

Figure 7.8 (cont'd). Temperature-dependent measured optical transmission intensity for mixture component (c) $x_{H\text{-}22.5}$ = 0.202, and (d) $x_{H\text{-}22.5}$ = 0.306 respectively in planar (open circle) cell and also homeotropic (closed square) cell configuration. Vertical arrows represent the corresponding phase transition.

system, the optical intensity value rapidly decreases prior to the transition to TGBA phase. However, it increases on entering the TGBA phase. On further cooling, the intensity drops down to a lower value at the transition to TGBC* phase for the mixtures except for the mixture $x_{H\text{-}22.5}$ = 0.306 in planar cell. This reduction in intensity is due to the mutual orientation of two orthogonal helix axes within the smectic blocks of this frustrated phase. Finally, the TGBC*–Sm-B*$_{hex}$ phase transition has been identified by a relatively small but continuous change in intensity for the mixture $x_{H\text{-}22.5}$ = 0.101 and also for the pure compound. However, it exhibit an abrupt change for the mixture $x_{H\text{-}22.5}$ = 0.202 and 0.306. The overall intensity for HG configuration has been found to be quite high than HT configuration for all of the investigated mixtures as well as for the pure compound. Hence, all of the phase transitions in the mixtures including the pure compound have clearly been detected and the related temperatures reveal a close agreement in accordance with the polarizing optical microscopy and DSC study.

7.6. Static dielectric parameters measurement

The temperature dependent parallel and perpendicular components of dielectric permittivity ($\varepsilon_{\parallel}$ and $\varepsilon_{\perp}$) have been measured by using Agilent 4294A impedance analyzer for the pure rod-like chiral compound along with all mixtures. By applying a signal voltage of 500 mV with a fixed frequency 10 kHz the dielectric parameters were recorded in both the HG and HT cell configurations. Following the values of both $\varepsilon_{\parallel}$ and $\varepsilon_{\perp}$, the average dielectric permittivity (ε_{avg}) along with the dielectric anisotropy ($\Delta\varepsilon = \varepsilon_{\parallel} - \varepsilon_{\perp}$) values have been determined throughout the whole mesomorphic region. Fig. 7.9(a) shows the dielectric parameters for the pure compound (2H6R) while Fig. 7.9(b-d) represents the same for mixtures $x_{H\text{-}22.5}$ = 0.101, 0.202, and 0.306 respectively.

It has been observed that the parallel component of permittivity ($\varepsilon_{\parallel}$) is higher than the perpendicular component ($\varepsilon_{\perp}$) in the vicinity of isotropic to N*

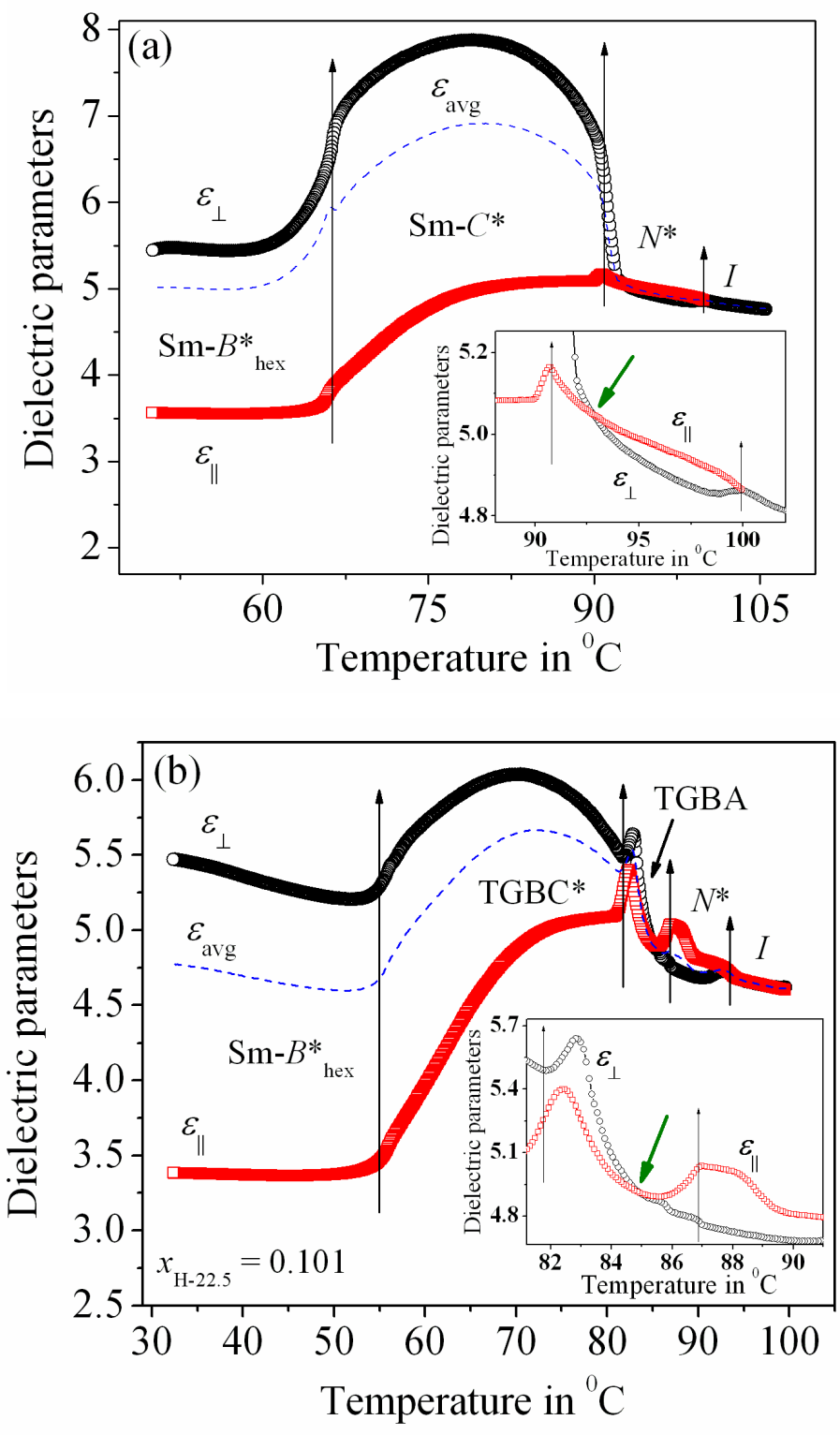

Figure 7.9. Temperature-dependent dielectric parameters ($\varepsilon_{\parallel}$, $\varepsilon_{\perp}$, ε_{avg}) for compound (a) 2H6R, (b) $x_{H\text{-}22.5}$ = 0.101 in planar or HG (open circle) cell and also homeotropic or HT (open square) cell configuration. Inset depicts the magnified version of permittivity inversion region. Vertical arrows represent the corresponding phase transition.

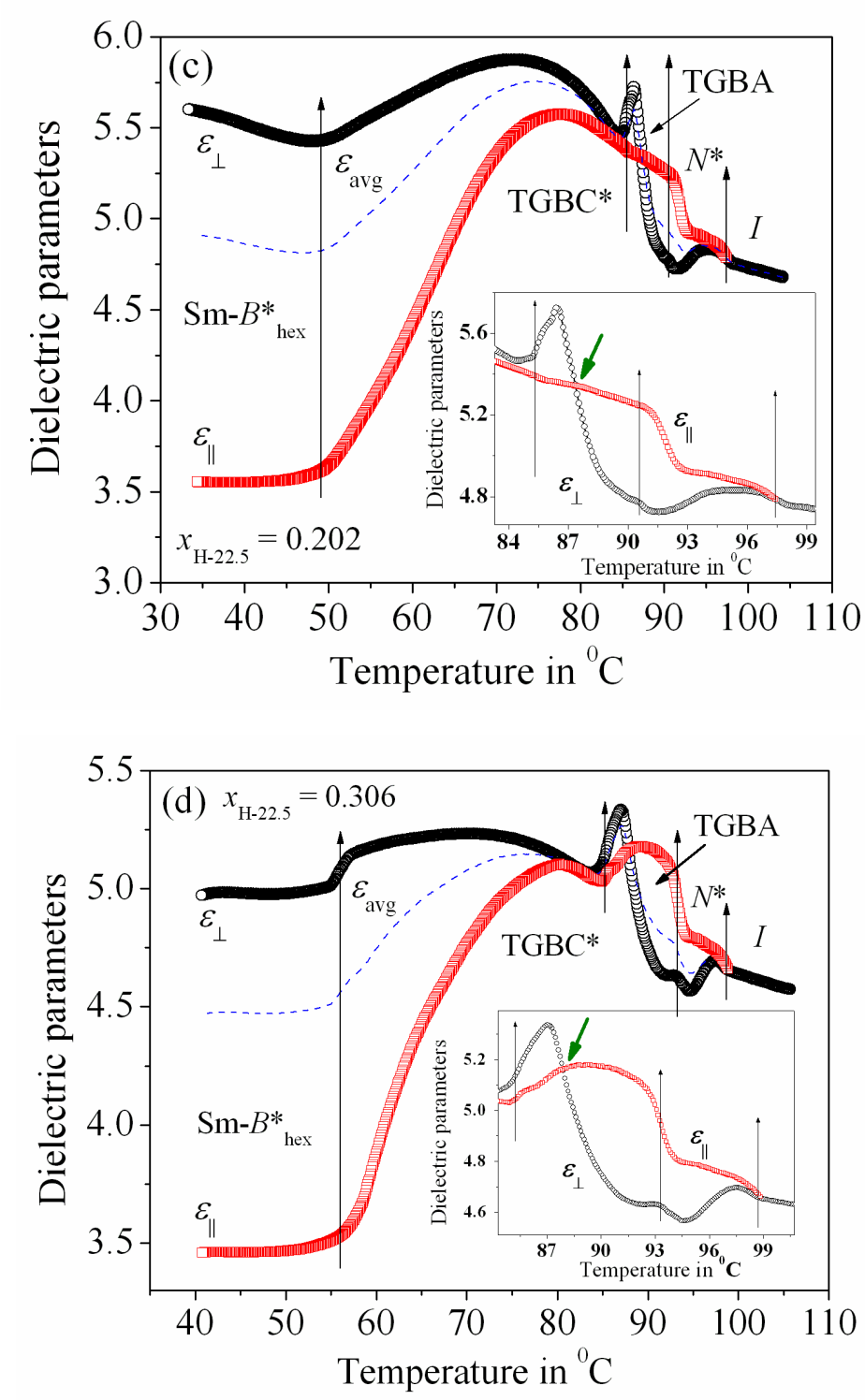

Figure 7.9 (cont'd). Temperature-dependent dielectric parameters ($\varepsilon_{\parallel}$, $\varepsilon_{\perp}$, ε_{avg}) for compound (c) $x_{H\text{-}22.5}$ = 0.202, (d) $x_{H\text{-}22.5}$ = 0.306 in planar or HG (open circle) cell and also homeotropic or HT (open square) cell configuration. Inset depicts the magnified version of permittivity inversion region. Vertical arrows represent the corresponding phase transition.

phase transition for all the investigated samples, specifying a positive value of the dielectric anisotropy ($\Delta\varepsilon$). On further cooling, the perpendicular component ($\varepsilon_{\perp}$) of permittivity in compound 2H6R represents a sharp augmentation in comparison to the parallel component ($\varepsilon_{\parallel}$) just prior to the transition from *N** to Sm-*C** phase. This type of quick enhancement of permittivity value at the transition is a characteristic gesture of Sm-*C** phase and it follows the temperature dependent Curie-Weiss law:

$$\varepsilon = \frac{C}{T_C - T} \tag{7.1}$$

where C is the Curie constant and T_C is the transition temperature. Consequently, the dielectric anisotropy data reveals a crossover from positive to negative value close to the *N**–Sm-*C** phase transition temperature and this particular inversion temperature (T_i) is marked with a green arrow in the inset of Fig. 7.9(a). Further decreasing the temperature, both the $\varepsilon_{\parallel}$ and $\varepsilon_{\perp}$ are initially found to increase gradually leading to the formation of a broad maximum within the Sm-*C** phase and then decreases slowly on approaching the low temperature Sm-B^*_{hex} phase, *i.e.*, it follows a convex type pattern in the Sm-*C** phase. Furthermore, a small but pronounce change in both the dielectric components has been observed at the transition to Sm-B^*_{hex} phase and remains more or less constant up to certain lower temperatures. Investigation on the dielectric parameters for the studied mixtures describes a similar kind of appearance for positive dielectric anisotropy in the cholesteric phase as shown in Fig. 7.9(b-d) and the sign inversion of the dielectric anisotropy ($\Delta\varepsilon$) value occurs in the TGBA phase. However, the variation of all the dielectric parameters with temperature in TGBC* phase has found to be almost identical as observed in the Sm-*C** phase for 2H6R compound. Moreover, in the Sm-B^*_{hex} phase, the magnitude of permittivity accomplishes a lower value in comparison to TGBC* phase and remains almost constant or slightly increases by lowering the temperature. The thermal variation of the dielectric anisotropy ($\Delta\varepsilon$) data for all the mixtures including the pure compound (2H6R) is depicted

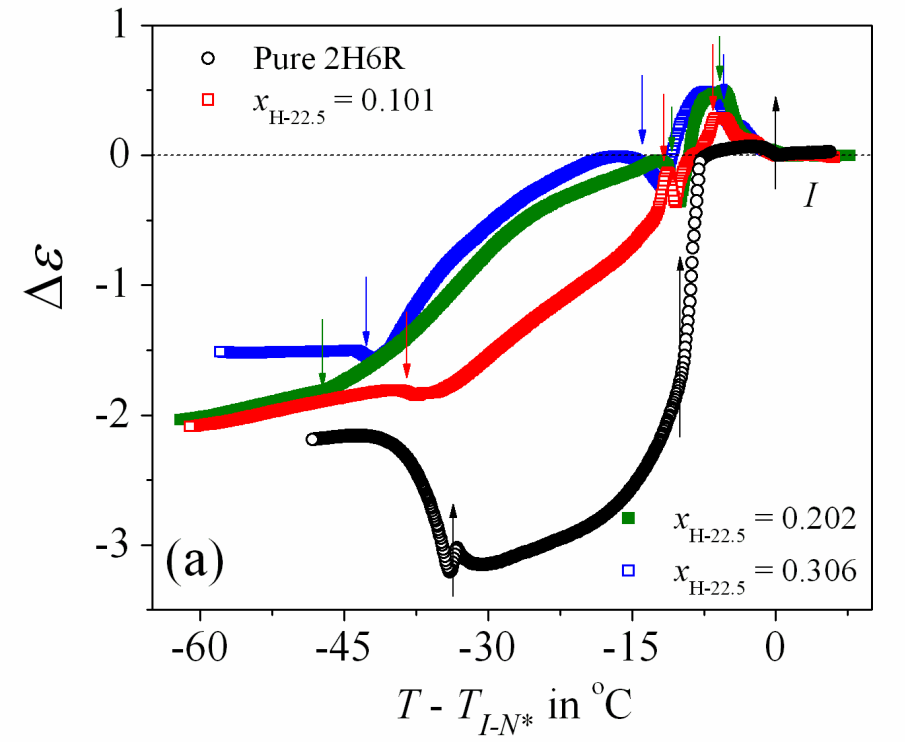

Figure 7.10. (a) Variation of dielectric anisotropy ($\Delta\varepsilon$) against the reduced temperature (T-$T_{I–N*}$). Vertical arrows represent the corresponding phase transition temperatures.

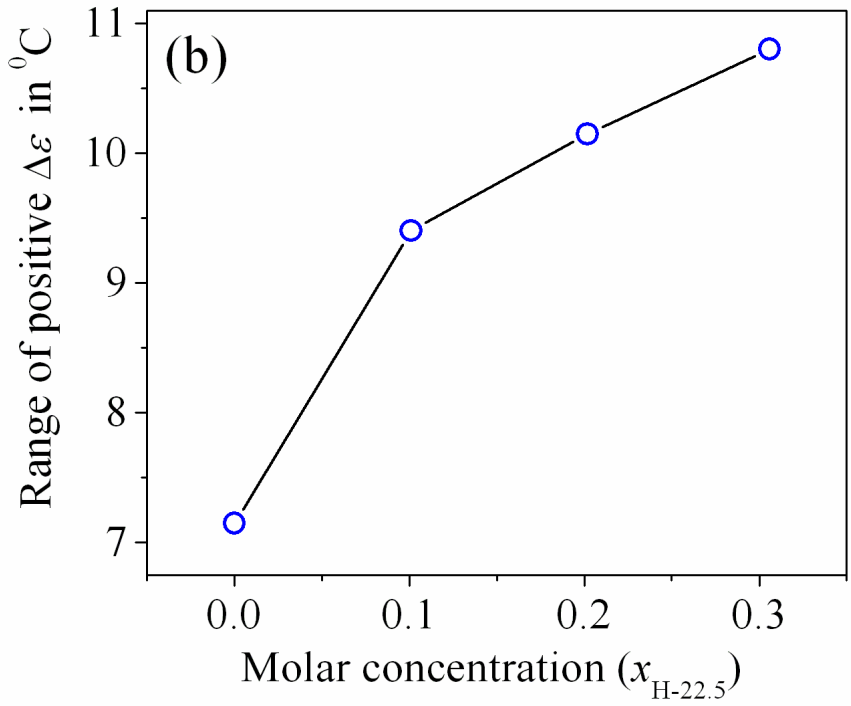

Figure 7.10. (b) The concentration variation of positive anisotropy ($\Delta\varepsilon$) range for all the mixture including the pure chiral 2H6R mesogen.

in Fig. 7.10(a). It is quite evident that the $\Delta\varepsilon$ always assumes a small positive value within the *N** phase and extend up to a certain temperature range of the TGBA phase. Although, the studied mixtures possess a negative value of the dielectric anisotropy in the TGBC* phase, the magnitude has found to increase by increasing the amount of bend-shaped compound. However, the $\Delta\varepsilon$ value is very low in the Sm-*C** phase for the pure compound. Surprisingly, the inversion temperature (T_i) of the dielectric anisotropy has a greater influence on the dopant concentration. In the present binary system, the inversion temperature reveals a large difference from the clearing temperature in accordance with the enhancement of the dopant concentration. As a result, the temperature range of the positive dielectric anisotropy region monotonically increases from a value of 7.15 ^{o}C for 2H6R to 10.44 ^{o}C for the mixture concentration $x_{H\text{-}22.5}$ = 0.306 as depicted in Fig. 7.10(b).

7.7. Spontaneous polarization study

The field induced spontaneous polarization (P_s) value for all the studied samples has been measured by field reversal polarization technique [81-83] in planar aligned ITO coated cell of thickness ~ 9 μm using a square wave as well as triangular wave AC input voltage (V_{pp} = 38V, f = 20Hz). In case of TGBC* phase, a single polarization peak has been detected in response to a triangular wave signal voltage and a current response hump appears in the square wave output voltage, indicating the TGBC* phase as a ferroelectric phase. Fig. 7.11 represents the measured value of P_s as a function of reduced temperature (T/T_C), where T_C is the corresponding TGBA–TGBC* phase transition temperature.

Investigation of Fig. 7.11 reveals that the value of P_s increases with decreasing the temperature and attains a maximum saturation value ~100 nC/Cm^2 at the Sm-*C** phase of the pure compound 2H6R, divulging a quite good agreement with the obtained value by Węgłowska *et al.*[59]. Such high value of polarization is due to the presence of the high tilt angle and strong

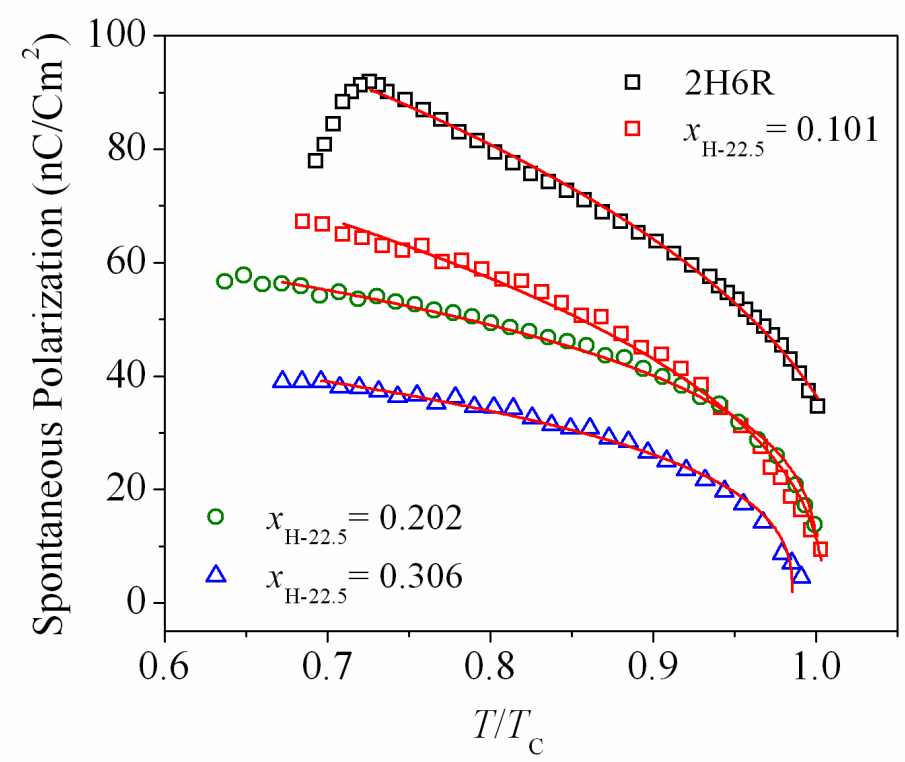

Figure 7.11. Value of spontaneous polarization (P_s) as a function of reduced temperature for pure compound (2H6R) and all the mixture components. The solid line is a fitting curve of Eq. (7.2).

alignment of the transverse dipole moments in the Sm-*C** phase. The increasing trend of spontaneous polarization values with decreasing temperature may be explained in terms of the reorientation of the dipoles and electrostatic interaction between the neighboring molecules. The induced TGBC* phases for the mixtures also exhibit a similar variation of polarization with decreasing temperature, having magnitude relatively smaller than that of the pure compound. The maximum value of P_s has found to be 68.4 nC/Cm^2, 57 nC/Cm^2 and 40 nC/Cm^2 for the mixture concentrations $x_{H\text{-}22.5}$ = 0.101, 0.202 and 0.306 respectively. Therefore, the effective value of P_s is reduced due to the introduction of achiral hockey stick-shaped compound in chiral mesogenic environment. It can be assumed that the mutual orientation of dipole moments for both the molecules is not favorable to each other in the mixtures and hence it reduces the value of spontaneous polarization. However, further increase in the dopant concentration, progressively suppresses the polarization value. The

weakening of core-core correlation between the dissimilar mesogenic compounds may affect the value of P_s [84-86]. Again the significant disparity in terminal chain length between the guest and host molecules may give rise to an influence on such decrease in P_s [87,88]. A similar type of decrease in spontaneous polarization value for a number of binary mixtures has been reported earlier [87].

In an attempt to verify the order nature of the TGBA–TGBC* phase transition the reduced temperature dependent polarization curves have been fitted with following expression [89,90]:

$$P_s = P_0(T_C - T)^{\beta} \tag{7.2}$$

where β is the critical exponent, both the P_0 and β are adjustable parameters and T_C represents the TGBA–TGBC* phase transition temperature. Fitted curves of Eq. (7.2) to the data points are shown in Fig. 7.11 as red lines whereas the fitted parameters are listed in Table 7.2. The extracted critical exponent β assumes a value 0.26±0.01 for the pure compound at the *N**–Sm-*C** phase transition. This value is very close to the tricritical mean field value (β = 0.25) indicating a weakly first order nature of the *N**–Sm-*C** phase transition [91]. Such type of first order transition from the *N** to Sm-*C** phase has also been reported in literature [92]. Furthermore, the value of β at the TGBA–TGBC* phase transition has found to be β = 0.28±0.02, 0.30±0.01 and

Table 7.2. Obtained fit parameter values from the fit to experimental P_S value with Eq. (7.2) for all of the mixtures including 2H6R compound.

$x_{H\text{-}22.5}$	P_0 in nC cm^{-2}	T_C in ^oC	β
0	22.61±0.52	90.09±0.37	0.26±0.01
0.101	17.28±0.89	82.14±0.14	0.28±0.02
0.202	21.31±0.81	85.67±0.13	0.30±0.01
0.306	13.55±0.75	83.55±0.16	0.33±0.02

0.33±0.02 for the mixture concentration $x_{H\text{-}22.5}$ = 0.101, 0.202 and 0.306 which shows an increasing pattern. Nevertheless, the related critical exponent β assumes a value 0.3125 predicted by the three-dimensional Ising model [91]. Here the critical exponent β for the mixtures $x_{H\text{-}22.5}$ = 0.202 and 0.306 are very close to the theoretically predicted value in 3-D Ising model, representing a second order nature of the TGBA–TGBC* phase transition. Accordingly, the obtained β values demonstrates that by increasing the hockey stick-shaped mesogen in the mixture, drives the weakly first order character of the *N**–Sm-*C** phase transition to the second order nature of the TGBA–TGBC* phase transition.

7.8. Response time and effective torsional bulk viscosity measurement

The response time (τ) for all the investigated mixtures along with the pure compound (2H6R) are portrayed in Fig. 7.12 against reduced temperature (T/T_C). In this system, the value of τ describes a monotonic enhancement

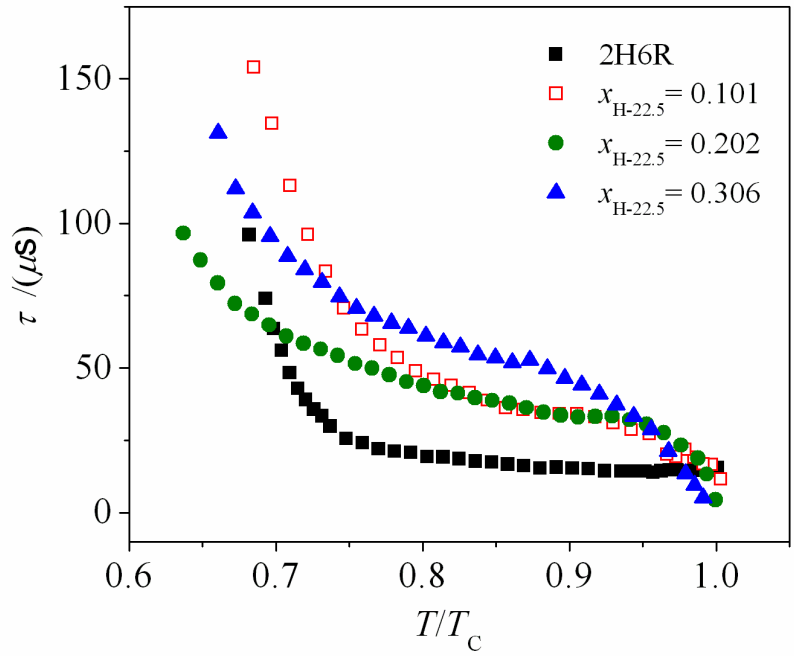

Figure 7.12. Reduced temperature dependent value of response time (τ) for pure compound (2H6R) including all the mixture components.

throughout the TGBC* phase by lowering the temperature. At a particular reduced temperature, all the mixtures possess a higher value of response time in comparison to that of the pure compound 2H6R. It signifies that due to the introduction of kink-shaped mesogen, effectively hinders the motion of the chiral center. Moreover, the mixture having molar concentration $x_{\text{H-22.5}} = 0.202$ divulges a slightly lower value ranging between 22–96 μs relative to other mixtures at lower temperature of the TGBC* phase. Probably the mutual interaction of divergent molecules is responsible to exhibit moderate τ value. Therefore, the studied mixtures having negative dielectric anisotropy in the TGBC* phase, exhibit a response time maximum up to τ_{max} ~152 μs are useful for the application in electro-optical devices.

The effective torsional bulk viscosity (η) is the necessary parameter to investigate the dynamical behavior of chiral LC compound, which is related to the rotational motion of the molecules around the twisted cone of the TGBC* or Sm-*C** phase. The variation of the effective torsional bulk viscosity with respect to reduced temperature (T/T_C) for all the mixtures including 2H6R compound are illustrated in Fig. 7.13 (a). A significant increasing pattern of the effective torsional bulk viscosity (η) has been observed by lowering the temperature and this trend is almost identical for all the mixtures including the pure compound as depicted in Figure 7.13(a). As the value of η is mostly depends upon the value of τ, the thermal variation exhibits almost similar pattern. However, all the investigated mixtures demonstrate slightly higher values of η relative to that of the pure chiral compound. Interestingly, although the value of η does not indicate any systematic variation with increasing achiral dopant concentration in the investigated mixtures, the magnitude of η achieve a maximum value of about 360 mPa S for the mixture concentration $x_{\text{H-22.5}} = 0.101$. As a result of the addition of the hockey stick-shaped mesogen into the chiral environment, such a variation of response time as well as torsional bulk viscosity can be described by Boulder model [93,94], according to which, the

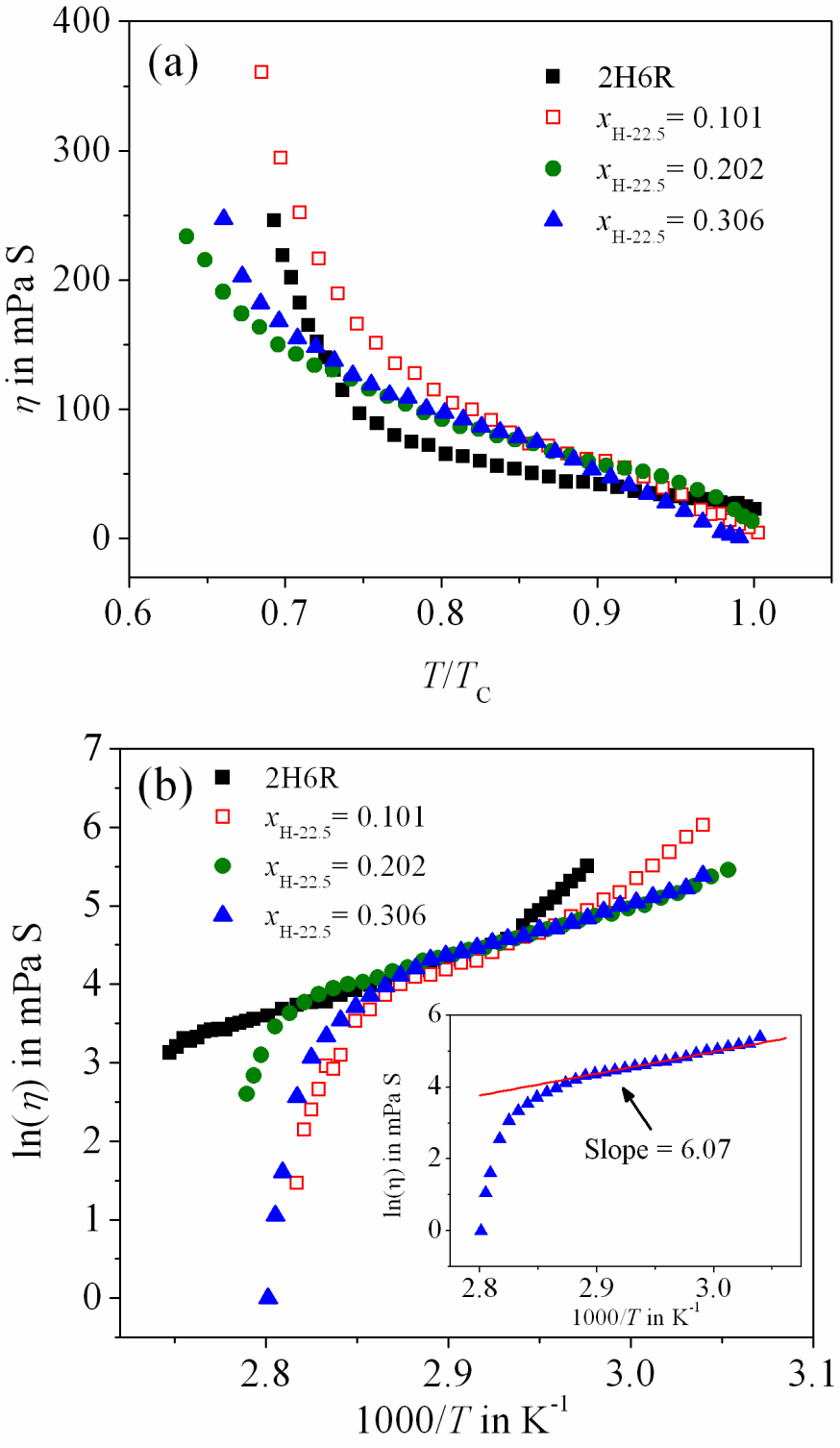

Figure 7.13. (a) Reduced temperature dependent value of effective torsional bulk viscosity (η) for all of the mixtures including the pure compound (2H6R). (b) Arrhenius plot of effective torsional bulk viscosity vs. (1000/T). Inset represents the linear fit to Eq. (7.3) to experimental data of $x_{H\text{-}22.5}$ = 0.306.

chiral molecules in the chiral-achiral system causes a modification in the orientational distributions of the transverse dipole moment of achiral molecules with regard to the polar C_2 axis. In fact, mutual core-core interactions of chiral and achiral components present in the mixtures may favor or oppose the orientation of the transverse dipole moment along the polar C_2 axis [84].

In an effort to determine the associated activation energy (E_a), the Arrhenius plot of effective torsional bulk viscosity has been plotted in Fig 7.13(b) for all of the mixtures along with the 2H6R compound and fitted with the following expression [95]:

$$\eta = \eta_0 \exp\left(\frac{E_a}{k_\beta T}\right) \tag{7.3}$$

where T is the absolute temperature and k_β is the Boltzmann's constant. A representative fit has been shown in the inset of Fig. 7.13(b) for the mixture concentration $x_{\text{H-22.5}}$ = 0.306. The slope of the linear region is calculated and further utilized to estimate the associated activation energy (E_a). The obtained values of E_a are found to be about 58 kJ/mole for pure 2H6R compound in Sm-*C** phase and 68.15 kJ/mole, 52.61 kJ/mole and 50.46 kJ/mole for the mixture concentrations $x_{\text{H-22.5}}$ = 0.101, 0.202 and 0.306 respectively in TGBC* phase. These experimental values of E_a are relatively higher than that of the reported values in mixtures having dissimilar molecular architectures [95].

7.9. Dielectric spectroscopy measurement

To recognize the frequency dependent molecular dynamics and their bulk properties associated with chiral phases (especially in frustrated TGB phases), the dielectric spectroscopy measurement has been performed in ITO coated HG (planar) cell for all the mixtures including the pure chiral compound. The frequency dependent real and imaginary parts (ε' and ε'') of the complex permittivity are shown in Fig. 7.14 (a-b) for the mixture component $x_{\text{H-22.5}}$ = 0.202 throughout the entire mesophase. In order to determine the relaxation frequency (f_R) and other dielectric parameters, the real and imaginary

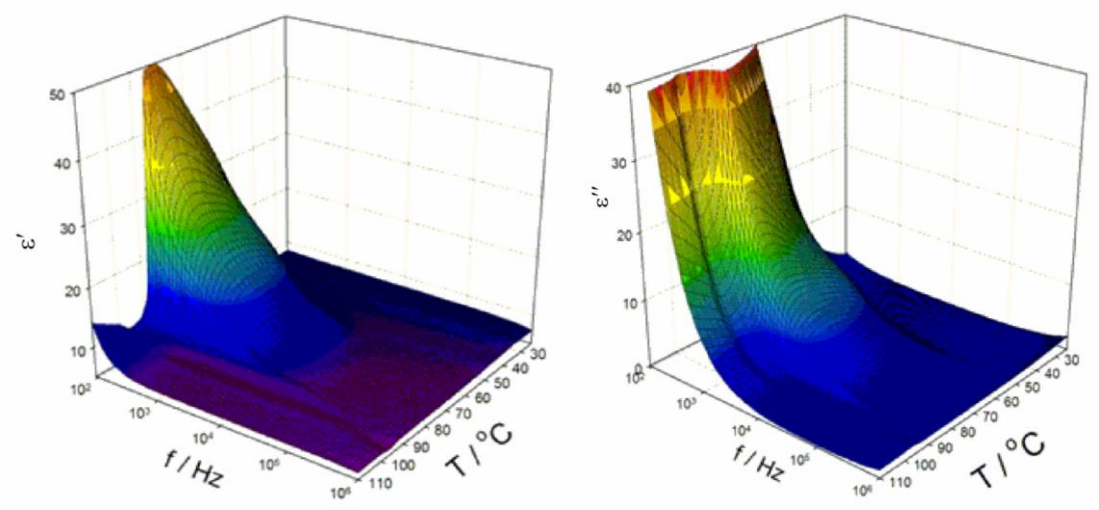

(a) (b)

Figure 7.14. 3D plot of (a) real (left side) and (b) imaginary (right-side) parts of complex permittivity versus temperature and frequency measured on cooling from the isotropic phase for the mixture component $x_{\text{H-22.5}} = 0.202$.

parts of the complex dielectric permittivity were fitted with the Havriliak-Negami (H-N) fitting functions [96-99] as described in chapter 2. The Arrhenius plots of relaxation frequency (f_R) and the variation of the dielectric strength ($\delta\varepsilon$) have been presented in Fig. 7.15(a,b) for pure 2H6R and one of the binary mixture $x_{\text{H-22.5}} = 0.202$ in Fig. 7.16(a,b) respectively.

Investigation on the relaxation parameters for pure compound (2H6R) (see Fig. 7.15) clearly describes a single characteristic relaxation mode in the *N** phase having a higher value of relaxation frequency of about ~1.2 MHz with a lower value of dielectric strength $\delta\varepsilon \sim 6$, though it increases by lowering the temperature at the *N**–Sm-*C** phase transition. However, the activation energy of this mode is 65.05 kJ/mole, which is a typical range for the *N**phase. As a consequence, this mode can be recognized as a soft mode of relaxation arises due to amplitude fluctuation of the polarization vector [100]. In case of Sm-*C** phase, another relaxation mode has appeared at the low-frequency region (~2.5 kHz) with a quite higher value of the dielectric strength ~18 compared to that of the *N** phase. Corresponding values of f_R and $\delta\varepsilon$ remains

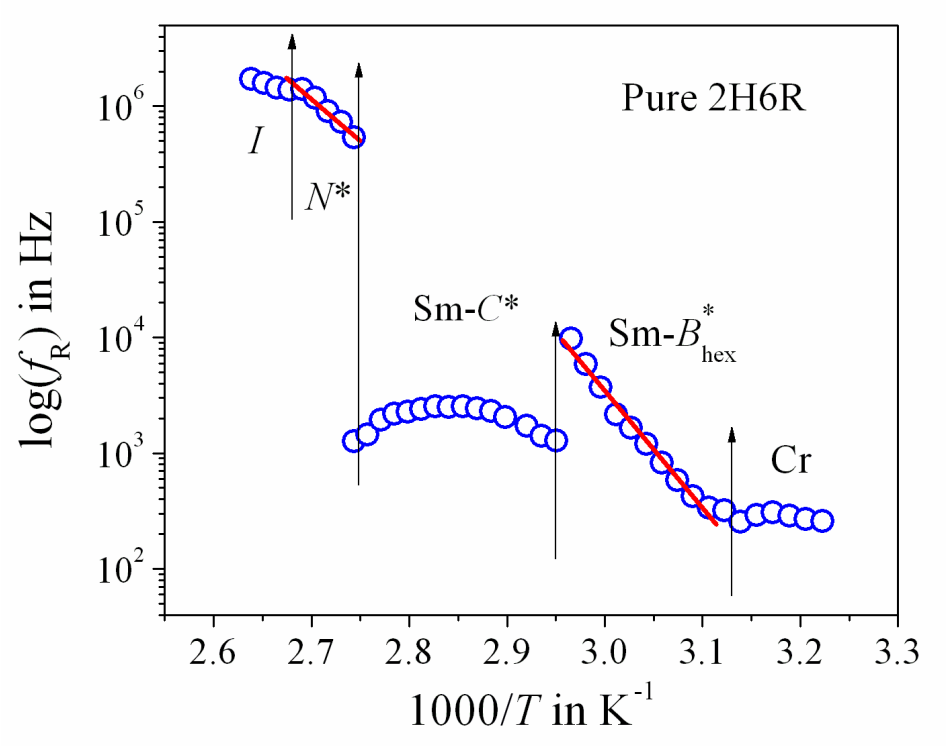

(a)

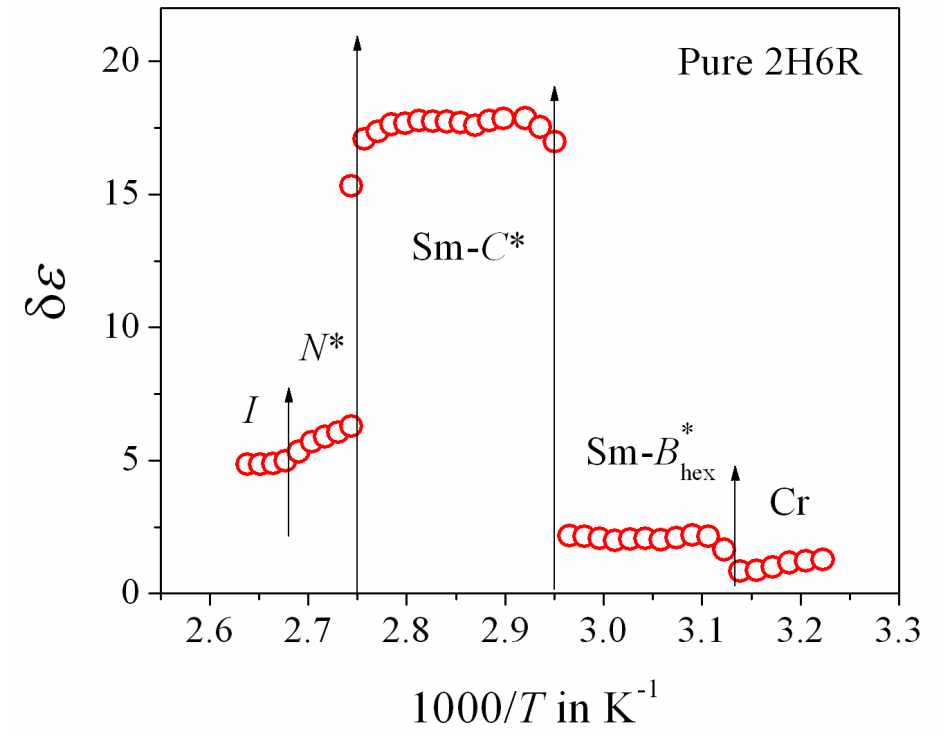

(b)

Figure 7.15. (a) Arrhenius plot of the relaxation frequency (f_R) and (b) the variation of dielectric strength ($\delta\varepsilon$) at different mesophases for the pure compound 2H6R.

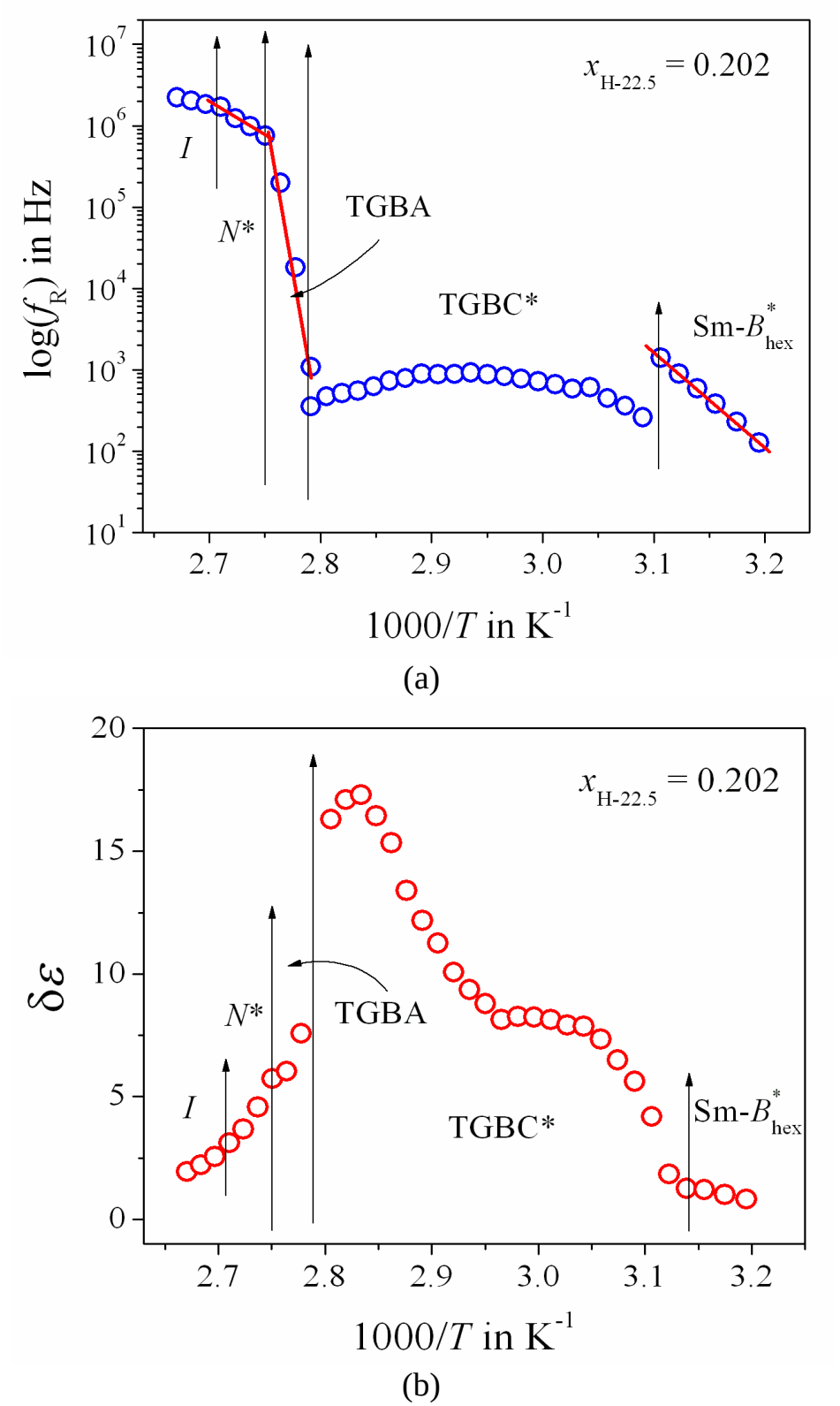

Figure 7.16. (a) Arrhenius plot of the relaxation frequency (f_R) and (b) the variation of dielectric strength ($\delta\varepsilon$) at different mesophases for the mixture concentration $x_{H\text{-}22.5}$ = 0.202.

almost constant throughout this mesophase region. Such a low-frequency relaxation phenomena manifests the phase fluctuations of the molecular director around the azimuthal orientation [101-104]. For the sake of convenience, this mode is ascribed as the Goldstone mode. Furthermore, it has been noticed that dielectric strength sharply increases near the *N**–Sm-*C** phase transition, which is the characteristics behavior of Sm-*C** phase and this enhancement follows the Curie-Weiss law (Eq. (7.1)). Furthermore, on entering to the Sm-B^*_{hex} phase, another relaxation mode appears at a moderate frequency of about ~10 KHz and monotonically decreases to lower frequency region by decreasing the temperature. Additionally, the dielectric strength is too low about 2.5 and remains constant throughout the mesophase. The activation energy of this mode is 85.52 kJ/mole. Consequently it can be assumed that this mode arises due to collective rotation of molecular director about their short axis [105]. Such weak relaxation mode can be expected for a hard type of smectic phase (Sm-B^*_{hex}) in which a rotational hinderence of the molecular director takes place around the long-axis due to the viscosity of the medium. A similar type of observations for the soft mode in *N** phase and Goldstone mode in Sm-*C** phase has been reported by Mishra *et al.* [106] and Wojciechoeski *et al.* [107] for two other chiral homologous compounds 4H3R and 1H3R respectively. Therefore our investigated results agreed well with the reported observations, but the only difference is to observe a higher value of dielectric strength in Sm-*C** phase. Relevance to this, the investigation of the dielectric modes in the binary mixtures demonstrates a similar type of soft mode relaxation in the *N** phase for all the concentrations (see Fig. 7.16 for $x_{H\text{-}22.5}$ = 0.202). Corresponding relaxation frequency (f_R) and the dielectric strength ($\delta\varepsilon$) of this mode are almost identical to that of pure 2H6R. The activation energy of this mode is about 71.59 kJ/mole, demonstrates a slightly higher value than that of the pure compound. However, all the mixtures reveals a similar kind of Goldstone mode in the TGBC* phase but have a relatively smaller value of relaxation frequency (~1.5 kHz) than the pure compound in

the Sm-*C** phase. The magnitude of the dielectric strength has found to be almost identical to that of the pure compound. On the other hand, the relaxation frequency in TGBA phase lies in between the soft mode and Goldstone mode, that seems like a transition from soft mode to Goldstone mode having greater activation energy of about 559.12 kJ/mole for the mixture $x_{\text{H-22.5}}$ = 0.202. Several experimental results on dielectric spectroscopy in TGBA [108-110] and TGBC* [111,112] phases have been reported earlier. It is anticipated that an electric field induces amplitude fluctuation of the tilt angle and hence a soft mode is visible in the TGBA phase. While in case of TGBC* phase, the phase fluctuation of the tilt angle leads to a Goldstone mode similar to the Sm-*C** phase. However, the present system divulges an Arrhenius type of relaxation mode in the TGBA phase, leading to a value of f_R which lies in between that of the soft mode and Goldstone mode. On the basis of spontaneous polarization measurement in the pure compound, the *N**–Sm-*C** phase transition exhibits a weakly first order nature, while due to the influence of hockey stick-shaped compound in the mixtures induces two intermediate TGB phases and drives the TGBA–TGBC* phase transition to a second order in nature. Moreover, the results from the investigation of relaxation phenomena suggest that the TGBA phase representing an intermediate state which defines a transition from a soft mode of *N** phase to a Goldstone mode of TGBC* phase. Furthermore, the low temperature Sm-B^*_{hex} phase exhibit the similar type of Arrhenius behavior of relaxation frequency for all the mixtures. This is due to the rotational hindrance of the molecular director around the long-axis. However, the activation energy for the low temperature Sm-B^*_{hex} phase is about 97.01 kJ/mole which is slightly higher than that of the pure compound.

7.10. Conclusion

The optical, dielectric and electro-optical properties have been carried out in the mesophases of a highly tilted ferroelectric chiral liquid crystal compound as well as in three binary mixtures with achiral hockey stick-shaped

compound H-22.5. Although the pure chiral 2H6R compound possess the phase sequence *I*–*N**–Sm-*C**–Sm-*B**$_{hex}$, two frustrated TGB phases (TGBA and TGBC*) have found to induced in between cholesteric (*N**) and Sm-*B**$_{hex}$ phases for all of the investigated mixtures. Both the TGB phases preliminary identified by optical textures as well as DSC study. Introduction of small quantity of hockey stick-shaped compound in binary mixtures is sufficient to perturb the helix of chiral compound and produces chiral twisted states (frustrated TGB phases) of higher pitch length. However, the temperature stability of such TGB phases has found to be a quite large range, but exhibit a non-linear dependency on the dopant concentration. Moreover, a sign inversion (positive to negative) of the dielectric anisotropy has been observed for all of the investigated mixtures including the pure compound and the corresponding inversion temperature signifies a remarkable influence on the dopant concentration. The obtained temperature range of the positive dielectric anisotropy region increases progressively by increasing the achiral hockey stick-shaped compound. Additionally, a significant decrease in the field induced spontaneous polarization value has been observed in the mixtures while the response time and effective torsional bulk viscosity exhibit a higher value than that of the pure compound. This is due to the influence of rotational hindrance of the molecules caused by the introduction of kink-shaped mesogen. Additionally, the obtained value of the exponent β suggesting that the mutual interaction between the two divergent molecules drives the weakly first order nature of the *N**–Sm-*C** phase in pure compound towards the second order nature of the TGBA–TGBC* phase transition. Investigation on dielectric spectroscopy reveals that the relaxation frequency and associated dielectric strength of the Goldstone mode in TGBC* phase slightly decreases with increasing the dopant concentration. However, the intermediate TGBA phase represents a transition from soft mode in *N** phase to a Goldstone mode in TGBC* phase with a greater value of activation energy. All such integral properties differing from the pure compound is due to the perturbation made by

the kink-shaped achiral molecule in the chiral-achiral system which opposes the inherent self-organized chiral properties of the pure ferroelectric compound. Consequently, the addition of bent-core molecule within a chiral environment essentially induces the TGB phases with negative dielectric anisotropy, reduces the spontaneous polarization value, and enhances the response time as well as the pitch length. Therefore, the appearances of such experimental results in the present binary system may facilitate clear understanding regarding the formation of quite stable TGB phases.

References:

[1] S.R. Renn, and T.C. Lubensky, *Phys. Rev. A*, **38**, 2132 (1988).

[2] J.W. Goodby, M.A. Waugh, S.M. Stein, E. Chin, R. Pindak, and J.S. Patel, *Nature*, **337**, 449 (1989).

[3] P.H. Martinot-Lagarde, *J. Phys.*, **37**, 129 (1976).

[4] M. Schadt, and W. Helfrich, *Appl. Phys. Lett.*, **18**, 127 (1971).

[5] G.W. Gray, and S.M. Kelly, *J. Mater. Chem.*, **9**, 2037 (1999).

[6] M. Klasen, M. Bremer, and K. Tarumi, *Jpn. J. Appl. Phys.*, **39**, L1180 (2000).

[7] Y. Ouchi, H. Takezoe, and A. Fukuda, *Jpn. J. Appl. Phys.*, **26**, 1 (1987).

[8] S.T. Lagerwall, in *Ferroelectric and antiferroelectric liquid crystals*, Wiley-VCH, New York (1999).

[9] N.A. Clark, and S.T. Lagerwall, *Appl. Phys. Lett.*, **36**, 899 (1980).

[10] H. Kawamto, *The history of liquid crystal displays*, *Proc. IEEE.*, **90**, 460 (2002).

[11] J.A. Castellano, *Liquid Crystals Today*, **1**, 1 (1991).

[12] D.M. Walba, E. Korblova, L. Eshdat, M. C. Biewer, H. Yang, C. Jones, M. Nakata, M. Talarico, R. Shao, and N. A. Clark, *Journal of the SID*, **15**, 585 (2007).

[13] D.K. Yang, and S.T Wu, in *Fundamentals of liquid crystal devices*, John Wiley & Sons Ltd., England (2006).

[14] B. Bahadur, in *Liquid crystals: applications and uses*, World Scientific, Singapore (1991).

[15] I. Inoi, in *Organofluorine chemistry, principles and commercial applications*, Plenum Press, New York (1994).

[16] S.M. Kelly, and M. O'Neill, in *Handbook of advanced electronic and photonic materials and devices*, Academic Press, London (2000).

[17] J.A. Castellano, in *Liquid gold: the story of liquid crystal displays and the creation of an industry*, World Scientific, Singapore (2005).

[18] P.P. Crooker, in *Blue Phases. Chirality in Liquid Crystals*, H.S. Kitzerow, C. Bahr, (Eds.), Springer, New York (2001).

[19] M. Nakata, Y. Takanishi, J. Watanabe, and H. Takezoe, *Phys. Rev. E*, **68**, 041710 (2003).

[20] T. Chan, C.W. Garland, and H.T. Nguyen, *Phys. Rev. E*, **52**, 5000 (1995).

[21] C. Ybert, L. Navailles, B. Pansu, F.Rieutord, H.T. Nguyen, and P. Barois, *Europhys. Lett.*, **63**, 840 (2003).

[22] H.-S. Kitzerow, in *Twist Grain Boundary Phases. Chirality in Liquid Crystals*; H.-S. Kitzerow, C. Bahr, (Eds.), Springer, New York (2001).

[23] I. Dierking, in *Textures of Liquid Crystals*, Wiley, Germany (2003).

[24] S.R. Renn, and T.C. Lubensky, *Mol. Cryst. Liq. Cryst.*, **209**, 349 (1991).

[25] J.W. Goodby, M.A. Waugh, S.M. Stein, E. Chin, R. Pindak, and J.S. Patel *J. Am. Chem. Soc.*, **111**, 8119 (1989).

[26] S.R. Renn, *Phys. Rev. A*, **45**, 953 (1992).

[27] W. Kuczynski, and H. Stegemeyer, *Mol. Cryst. Liq. Cryst.*, **260**, 377 (1995).

[28] O.D. Lavrentovich, Y.A. Nastishin, V.I. Kulishov, Y.S. Narkevich, and A.S. Tolochko, *Europhys. Lett.*, **13**, 313 (1990).

[29] S.K. Prasad, V.N. Raja, G.G. Nair, and J.W. Goodby, *Mol. Cryst. Liq. Cryst.*, **250**, 239 (1994).

[30] C.J. Booth, J.W. Goodby, J.P. Hardy, and K.J. Toyne, *Liq. Cryst.*, **16,** 43 (1994).

[31] Y. Sah, *Mol. Cryst. Liq. Cryst.*, **302**, 207 (1997).

[32] H. Ocak, B. Bilgin-Eran, D. Guzeller, M. Prehm, and C. Tschierske, *Chem. Commun.*, **51**, 7512 (2015).

[33] V. Punjani, G. Mohiuddin, S. Kaur, R.K. Khan, S. Ghosh, and S.K. Pal, *Chem. Commun.*, **54**, 3452 (2018).

[34] T. Seikine, T. Niori, M. Sone, J. Watanabe, S.W. Choi, Y. Takanashi, and H. Takezoe, *Jpn. J. Appl. Phys.*, **36**, 6455 (1997).

[35] G. Pelzl, S. Diele, and W. Weissflog, *Adv. Mater.*, **11**, 707 (1999).

[36] K.J.K. Semmler, T.J. Dingemans, and E.T. Samulski, *Liq. Cryst.*, **24**, 799 (1998).

[37] A. Eremin, S. Diele, G. Pelzl, H. Nádasi, W. Weissflog, J. Salfetnikova, and H. Kresse, *Phys. Rev. E*, **64**, 051707 (2001).

[38] T. Sekine, T. Takanishi, T. Niori, J. Watanabe, and H. Takezoe, *Jpn. J. Appl. Phys.*, **36**, 1201 (1997).

[39] D. Link, G. Natale, R. Shao, J.E. Maclennan, N.A. Clark, E. Korblova, and D.M. Walba, *Science*, **278**, 1924 (1997).

[40] J. Harden, B. Mbanga, N. Éber, K. Fodor-Csorba, S. Sprunt, J.T. Gleeson, and A. Jákli, *Phys. Rev. Lett.*, **97**, 157802 (2006).

[41] J. Harden, R. Teeling, J.T. Gleeson, S. Sprunt, and A. Jákli, *Phys. Rev. E*, **78**, 031702 (2008).

[42] C. Bailey, K. Fodor-Csorba, J.T. Gleeson, S.N. Sprunt, and A. Jákli, *Soft Matter*, **5**, 3618 (2009).

[43] E. Dorjgotov, K. Fodor-Csorba, J.T. Gleeson, S. Sprunt, and A. Jákli, *Liq. Cryst.*, **35**, 149 (2008).

[44] S. Dhara, F. Araoka, M. Lee, K.V. Le, L. Guo, B.K. Sadashiva, K. Song, K. Ishikawa, and H. Takezoe, *Phys. Rev. E*, **78**, 050701 (2008).

[45] D. Wiant, J. T. Gleeson, N. Éber, K. Fodor-Csorba, A. Jákli, and T. Tóth-Katona, *Phys. Rev. E*, **72**, 041712 (2005).

[46] S. Tanaka, S. Dhara, B.K. Sadashiva, Y. Shimbo, Y. Takanishi, F. Araoka, K. Ishikawa, and H. Takezoe, *Phys. Rev. E*, **77**, 041708 (2008).

[47] S. Tanaka, H. Takezoe, N. Éber, K. Fodor-Csorba, A. Vajda, and A. Buka, *Phys. Rev. E*, **80**, 021702 (2009).

[48] M. Alaasar, M. Prehm, S. Poppe, and C. Tschierske, *Chem. Eur. J.*, **23**, 5541 (2017).

[49] N. Sebastian, S. Belau, A. Eremin, M. Alaasar, M. Prehm, and C. Tschierske, *Phys. Chem. Chem. Phys.*, **19**, 5895 (2017).

[50] D. Guzeller, H. Ocak, B.B. -Eran, M. Prehm, and C. Tschierske, *J. Mater. Chem. C*, **3**, 4269 (2015).

[51] F.C. Yu, and L.J. Yu, *Chem. Mater*., **18**, 5410 (2006).

[52] F.C. Yu, and L.J. Yu, *Liq. Cryst*., **35**, 799 (2008).

[53] R. Stannarius, J. Li, and W. Weissflog, *Phys. Rev. Lett*., **90**, 025502 (2003).

[54] S.T. Wang, S.L. Wang, X.F. Han, Z.Q. Liu, S. Findeisen, W. Weissflog, and C.C. Huang, *Liq. Cryst*., **32**, 609 (2005).

[55] B. Das, A. Pramanik, M.K. Das, A. Bubnov, V. Hamplova, and M. Kašpar, *J. Mol. Struct.*, **1013**, 119 (2012).

[56] M. Nakata, Y. Takanishi, J. Watanabe, and H. Takezoe, *Phys. Rev. E*, **68**, 041710 (2003).

[57] S. Taushanoff, K. Van Le, J. Williams, R.J. Twieg, B. K. Sadashiva, H. Takezoe, and A. Jakli, *J. Mater. Chem.*, **20**, 5893 (2010).

[58] V. Novotná, M. Glogarová, V. Kozmík, J. Svoboda, V. Hamplová, M. Kašpar, and D. Pociecha, *Soft Matter*, **9**, 647 (2013).

[59] D. Węgłowska, and R. Dąbrowski, *Liq. Cryst.*, **41**, 1116 (2014).

[60] A. Chakraborty, B. Das, M.K. Das, S. Findeisen-Tandel, M. -G. Tamba, U. Baumeister, H. Kresse, and W. Weissflog, *Liq. Cryst.*, **38**, 1085 (2011).

[61] A. Chakraborty, M.K. Das, B. Das, U. Baumeister, and W. Weissflog, *J. Mater. Chem. C*, **1**, 7418 (2013).

[62] I. Dierking, F. Giesselmann, P. Zugenmaier, W. Kuczynskit, S.T. Lagerwall, and B. Stebler, *Liq. Cryst.*, **13**, 45 (1993).

[63] E. Sackmann, S. Meiboom, L.C. Snyder, A.E. Meixner, and R.E. Dietz, *J. Am. Chem. Soc.*, **90**, 3567 (1968).

[64] F.D. Saeva, and J. Wysocki, *J. Am. Chem Soc.*, **93**, 5928 (1971).

[65] H. Finkelmann, and H. Stegemeyer, *Z. Naturforsch.*, **28a**, 799 (1973).

[66] A. J. Slaney, I. Nishiyama, P. Styring, and J.W. Goodby, *J. Mater. Chem.*, **2**, 805 (1992).

[67] I. Dierking, F. Giesselmann, P. Zugenmaier, K. Mohr, H. Zaschke, and W. Kuczynski, *Z. Naturforsch.*, **49a**, 1081 (1994).

[68] I. Dierking, and S.T. Lagerwall, *Liq. Cryst.*, **26**, 83 (1999).

[69] P. Archer, and I. Dierking, *Liq. Cryst.*, **33**, 257 (2006).

[70] W. Kuczynski, and H. Stegemeyer, *SPIE*, **3318**, 90 (1997).

[71] W. Kuczynski, in *Self-organization in Chiral Liquid Crystals*, W. Kuczynski (ed.), Scientific, Poznan (1997).

[72] P.A. Pramod, R. Pratibha, and N.V. Madhusudana, *Current Science*, **73**, 761 (1997).

[73] Y. Galerne, *J. Phys. France II*, **4**, 1699 (1994).

[74] V. Novotná, M. Glogarová, V. Kozmik, J. Svoboda, V. Hamplová, M. Kašpar, and D. Pociecha, *Soft Matter*, **9**, 647 (2013).

[75] R. Dhar, *Phase Transit.*, **79**, 175 (2006).

[76] I. Dierking, *Liq. Cryst.*, **28**, 165 (2001).

[77] A. Saipa, and F. Giesselmann, *Liq. Cryst.*, **29**, 347 (2002).

[78] G. Sarkar, M.K. Das, R. Paul, B. Das, and W. Weissflog, *Phase Transit.*, **82**, 433 (2009).

[79] T. Scharf, in *Polarized Light in Liquid Crystals and Polymers*, Wiley, Hoboken, NJ, (2007).

[80] A. Prasad, and M.K. Das, *J. Phys.: Condens. Matter*, **22**, 195106 (2010).

[81] K. Miyasato, S. Abe, H. Takezoe, A. Fukuda, and E. Kuze, *Jpn. J Appl. Phys.*, **22**, L661 (1983).

[82] A. Pramanik, M.K. Das, B. Das, M. Żurowska, and R. Dabrowski, *Liq. Cryst.*, **42**, 412 (2015).

[83] S.S. Bawa, A.M. Biradar, K. Saxena, and S. Chandra, *Rev. Sci. Instrum.*, **59**, 2023 (1988).

[84] R.P. Lemieux, *Chem. Soc. Rev.*, **36**, 2033 (2007).

[85] R.P. Lemieux, *Acc. Chem. Res.*, **34**, 845 (2001).

[86] D. Vizitiu, C. Lazar, B.J. Halden, and R.P. Lemieux, *J. Am. Chem. Soc.*, **121**, 8229 (1999).

[87] S. Jaradat, N.W. Roberts, Y. Wang, L.S. Hirst, and H.F. Gleeson, *J. Mater. Chem.*, **16**, 3753 (2006).

[88] M.P. Thompson, and R.P. Lemieux, *J. Mater. Chem.*, **17**, 5068 (2007).

[89] J.W. Goodby, J.S. Patel, and E. Chin, *J. Phys. Chem.*, **91**, 5151 (1987).

[90] A.D.L. Chandani, T. Hagiwara, Y. Suzuki, Y. Ouchi, H. Takezoe, and A. Fukuda, *Jpn. J. Appl. Phys.*, **27**, L729 (1988).

[91] H. Yurtseven, and D. Kavruk, *Ferroelectrics*, **367**, 190 (2008).

[92] A. Mikułko, M. Marzec, M.D. Ossowska-Chruściel, J. Chruściel, and S. Wróbel, *Ferroelectrics*, **343**, 209 (2006).

[93] D.M. Walba, in *Advances in the Synthesis and Reactivity of Solids*, T.E. Mallouk (Ed.), Vol.1, JAI Press Ltd. Greenwich (1991).

[94] D.M. Walba, and N.A. Clark, *Proc. SPIE, Spatial Light Modulators and Applications II*, **0825**, 81 (1988).

[95] J. Hemine, A. Daoudi, M. Zazoui, C. Legrand, N. Isaert, A. Elkaaouachi, and H.T. Nguyen, *Spectrosc. Lett.*, **41**, 285 (2008).

[96] S. Havriliak, and S. Negami, *Polymer* **8**, 161 (1967).

[97] S. Havriliak, and S. Negami, *J. Poly. Sci.* **14**, 99 (1966).

[98] P. Nayek, S. Ghosh, S. Roy, T. P. Majumder, and R. Dabrowski, *J. Mol. Liq.*, **175**, 91 (2012).

[99] S. Ghosh, P. Nayek, S. K. Roy, T. P. Majumder, and R. Dabrowski, *Liq. Cryst.*, **37**, 369 (2010).

[100] R. Dabrowski, *Liq. Cryst.*, **42**, 783 (2015).

[101] A. Mishra, M. Zurowska, R. Dabrowski, and R. Dhar, *Phase Transit.*, **87**, 746 (2014).

[102] A. Levstik, T. Carlsson, C. Filipič, I. Levstik, and B. Žekš, *Phys. Rev. A*, **35**, 3527 (1987).

[103] P.K. Mandal, B.R. Jaishi, W. Hasse, R. Dabrowski, M. Tykarska, and P. Kula, *Phase Transit.*, **79**, 223 (2006).

[104] S. Haldar, K.C. Dey, D. Sinha, P.K. Mandal, W. Hasse, and P. Kula, *Liq. Cryst.*, **39**, 1196 (2012).

[105] M.B. Pandey, S.K. Pandey, U.B. Singh, R. Dhar, M. Tykarska, and R. Dabrowski, *Liq. Cryst.*, **41**, 1879 (2014).

[106] A. Mishra, D. Węgłowska, R. Dąbrowski, and R. Dhar, *Liq. Cryst.*, **42**, 1543 (2015).

[107] M. Wojciechoeski, G. W. Bak, and M. Tykarska, *Scientific Bulletin of the Lodz University of Technology*, **36**, 77 (2015).

[108] C. Girold, C. Legrand, N. Isaert, P. Pochat, J.P. Parneix, H.T. Nguyen, and C. Destrade, *Ferroelectrics*, **147,** 171 (1993).

[109] H. Xu, Y.P. Panarin, J.K. Vij, A.J. Seed, M. Hird, and J.W. Goodby, *J. Phys.: Condens. Matter*, **7,** 7443 (1995).

[110] S. Wrobel, S. Hiller, M. Pfeiffer, M. Marzec, and W, Haase, *Liq. Cryst.*, **18,** 21 (1995).

[111] F. Bougrioua, N. Isaert, C. Legrand, A. Bouchta, P. Barois, and H.T. Nguyen, *Ferroelectrics*, **180**, 35 (1996).

[112] M. Ismaili, F. Bougrioua, N. Isaert, C. Legrand, and H.T. Nguyen, *Phys. Rev. E*, **65**, 11701 (2001).